AD-A043 420 LOCKHEED MISSILES AND SPACE CO INC PALO ALTO CALIF PA--ETC F/G 4/1
FURTHER EVALUATION OF ICECAP AURORAL 4.3 MICROMETERS ZENITH RAD--ETC(U)
OCT 76 J B KUMER DNA001-76-C-0015

UNCLASSIFIED LMSC/D554539 DNA-4260F NL

| OF |
AD
A043420

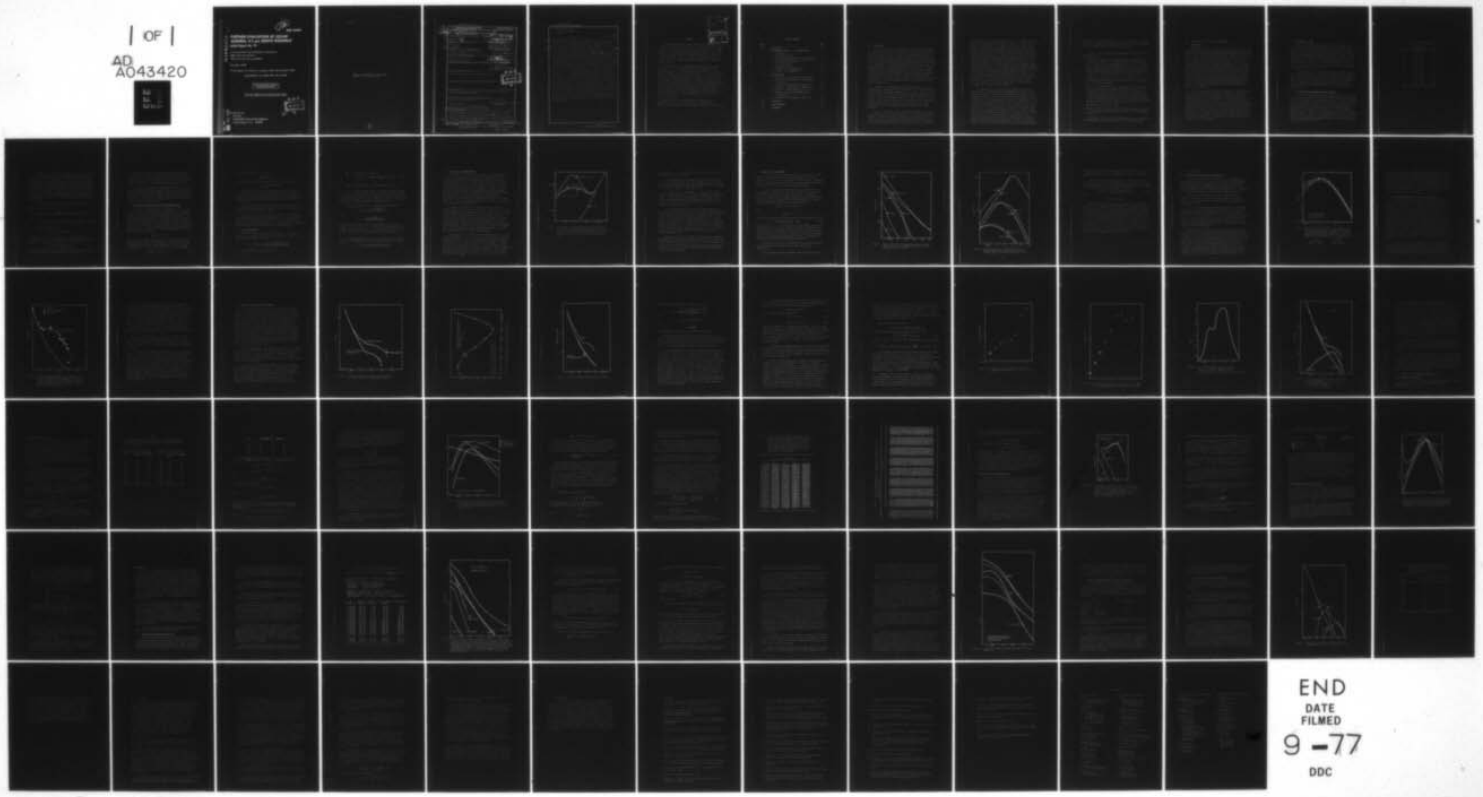

END
DATE FILMED
9 -77
DDC

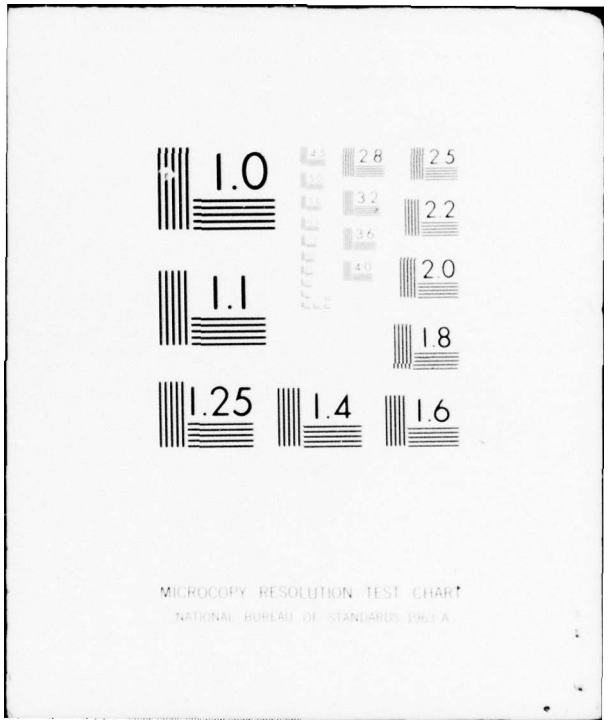
1.0
1.1
1.25
1.4
1.6
2.8
2.5
3.2
2.2
3.6
2.0
4.0
1.8
MICROCOPY RESOLUTION TEST CHART
NATIONAL BUREAU OF STANDARDS 1963-A

DNA 4260F

FURTHER EVALUATION OF ICECAP AURORAL 4.3 μm ZENITH RADIANCE

HAES Report No. 57

Lockheed Palo Alto Research Laboratory
3251 Hanover Street
Palo Alto, California 94304

October 1976

Final Report for Period 1 August 1975—31 October 1976

CONTRACT No. DNA 001-76-C-0015

APPROVED FOR PUBLIC RELEASE;
DISTRIBUTION UNLIMITED.

THIS WORK SPONSORED BY THE DEFENSE NUCLEAR AGENCY
UNDER RDT&E RMSS CODE B322076464 S99QAXHI00421 H2590D.

Prepared for
Director
DEFENSE NUCLEAR AGENCY
Washington, D. C. 20305

Destroy this report when it is no longer
needed. Do not return to sender.

UNCLASSIFIED

SECURITY CLASSIFICATION OF THIS PAGE (When Data Entered)

REPORT DOCUMENTATION PAGE	READ INSTRUCTIONS BEFORE COMPLETING FORM
1. REPORT NUMBER: DNA 4260F, HAES-57	2. GOVT ACCESSION NO. / 3. RECIPIENT'S CATALOG NUMBER
4. TITLE (and Subtitle): FURTHER EVALUATION OF ICECAP AURORAL 4.3 μm ZENITH RADIANCE. HAES Report Number 57.	5. TYPE OF REPORT & PERIOD COVERED: Final Report for Period 1 Aug 75—31 Oct 76
	6. PERFORMING ORG. REPORT NUMBER: LMSC D554539
7. AUTHOR(s): J. B. Kumer	8. CONTRACT OR GRANT NUMBER(s): DNA 001-76-C-0015
9. PERFORMING ORGANIZATION NAME AND ADDRESS: Lockheed Palo Alto Research Laboratory, 3251 Hanover Street, Palo Alto, California 94304	10. PROGRAM ELEMENT, PROJECT, TASK AREA & WORK UNIT NUMBERS: NWED Subtask S99QAXHI004-21
11. CONTROLLING OFFICE NAME AND ADDRESS: Director, Defense Nuclear Agency, Washington, D.C. 20305	12. REPORT DATE: October 1976 / 13. NUMBER OF PAGES: 78 (12 77p.)
14. MONITORING AGENCY NAME & ADDRESS (if different from Controlling Office)	15. SECURITY CLASS (of this report): UNCLASSIFIED / 15a. DECLASSIFICATION/DOWNGRADING SCHEDULE

16. DISTRIBUTION STATEMENT (of this Report)

Approved for public release; distribution unlimited.

DDC RECEIVED AUG 25 1977 C

17. DISTRIBUTION STATEMENT (of the abstract entered in Block 20, if different from Report)

18. SUPPLEMENTARY NOTES

This work sponsored by the Defense Nuclear Agency under RDT&E RMSS Code B322076464 S99QAXHI00421 H2590D.

19. KEY WORDS (Continue on reverse side if necessary and identify by block number)

Nuclear Optical Interference
CO_2 4.3 μm Aurora
Nuclear Enhanced 4.3 μm Atmospheric Emissions
CO_2 4.3 μm Airglow
Time Dependent Radiative Transport Theory

20. ABSTRACT (Continue on reverse side if necessary and identify by block number)

The author has successfully developed the numerical facility to solve the exact time dependent plane parallel radiation transport equations which describe 4.3 μm emission in the upper atmosphere. He found that accurate modeling for high altitude CO_2 4.3 μm emissions requires that the effects of the weak CO_2 4.3 μm bands are included in the calculation. He used our

DD FORM 1 JAN 73 1473 EDITION OF 1 NOV 65 IS OBSOLETE

210118

UNCLASSIFIED

SECURITY CLASSIFICATION OF THIS PAGE (When Data Entered)

19. KEY WORDS (Continued)

$N_2^{\ddagger}$ Vibration Relaxation Time

ICECAP

20. ABSTRACT (Continued) (fr p 1473A)

improved facility for assessment of 4.3 μm zenith radiance data obtained 24 March 1973 and found that somewhat better agreement with these data were obtained in the altitude region z < 90 km than we had previously reported. It was the inclusion of the weak CO_2 (ν_3) bands which resulted in obtaining a better fit to these data in the region z < 90 km. A 4.3 μm zenith radiance component which has its maximum at z ≈ 80 km appears in the 4.3 μm zenith radiance data obtained on 11 April 1974 and 27 March 1973 under quiet aurora conditions and also perhaps in the 25 February 1974 up-leg data obtained in the edge of a discrete arc. We established that these features may be evidence for a 4.3 μm airglow layer due to the process $OH(v) + N_2 \xrightarrow{VV} OH(v-1) + N_2^{\ddagger}$, $N_2^{\ddagger} + CO_2 \underset{\leftarrow}{\overset{VV}{\rightarrow}} N_2 + CO_2(\nu_3)$, $CO_2(\nu_3) \rightarrow CO_2 + h\nu(4.3\ \mu m)$. About 0.06 to 0.22 ergs/cm^2 sec $N_2^{\ddagger}$ excitation is required. We developed a facility to use the ground based photometric data on the history of auroral emissions at 6300 Å (red) and at 4278 Å or 3914 Å (blue) in order to generate the time history of the altitude dependence of energy deposit q(z,t) by particle precipitation. We successfully applied this facility for analysis of auroral 4.3 μm data obtained 25 February 1974. We showed that the data obtained in 2 rocket flights 6 March 1975 under conditions of a sunlit and dark atmosphere respectively can be consistently explained on the basis of two CO_2 4.3 μm airglow mechanisms. One is the absorption of sunlight at 4.3 and 2.7 μm by CO_2 followed by re-emission at 4.3 μm which is operative in the sunlit twilight case. The other is the $OH(v) \xrightarrow{VV} N_2$ mechanism which is operative in the ratio 1:3 in the sunlit and dark cases respectively.

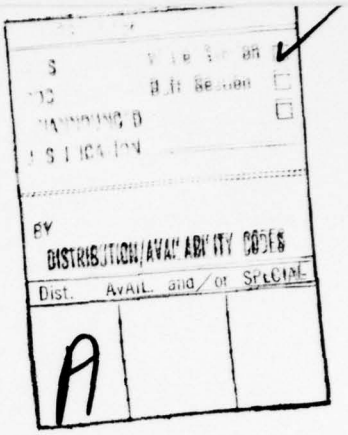

PREFACE

The High Altitude Effects Simulation (HAES) Program sponsored by the Defense Nuclear Agency since the early 1970 time period, compromises several groupings of separate, but interrelated technical activities, e.g., ICECAP (Infrared Chemistry Experiments-Coordinated Auroral Program). Each of the latter have the common objectives of providing information ascertained as essential for the development and validation of predictive computer codes designed for use with high priority DoD radar, communications, and optical defensive systems.

Since the inception of the HAES Program, significant achievements and results have been described in reports published by DNA, participating service laboratories, and supportive organizations. In order to provide greater visibility for such information and enhance its timely applications, significant reports published since early calendar 1974 shall be identified with an assigned HAES serial number and the appropriate activity acronym (e.g., ICECAP) as part of the report title. A complete and current bibliography of all HAES reports issued prior to and subsequent to HAES Report No. 1, dated 5 February 1974 entitled, "Rocket Launch of an SWIR Spectrometer into an Aurora (ICECAP 72)," AFCRL Environmental Research Paper No. 466, is maintained and available on request from DASIAC, DoD Nuclear Information and Analysis Center, 816 State Street, Santa Barbara, California, 93102, Telephone [805] 965-0551.

This report, which is the final report under DNA Contract No. DNA001-76-C-0015 is the fifty seventh report in the HAES series. It documents work performed in the period 1 August 1975 through 31 October 1976.

TABLE OF CONTENTS

1.0 INTRODUCTION

The long range purpose of our project is to develop general capability to predict upper atmospheric optical nuclear effects near 4.3 μm for exoatmospheric detonations. Enhanced 4.3 μm and other infrared upper atmospheric emissions are expected to result from the enhanced energy deposit in the upper atmosphere which results from an exospheric detonation. Obvious mechanisms by which these detonations deposit energy into the upper atmosphere include x-rays, debris, β radiation, and nuclear induced current systems and shock waves. At high latitudes there occur natural mechanisms for energy deposit in the upper atmosphere which are remarkably similar to the nuclear mechanisms. Amongst these natural mechanisms are included energy deposit by particle precipitation and also Joule heating associated with the large westward flowing current systems which exist in the high latitude ionosphere in the midnight to 6 o'clock local time zone. The visible auroras observed at high latitudes result from particle precipitation.

A purpose of the DNA/AFGL auroral measurements program is to measure simultaneously the upper atmospheric energy deposit by these natural mechanisms and the resultant enhancements in upper atmospheric infrared emissions. It is our job to provide a theory which uses the energy deposit measurements as input in order to predict enhanced upper atmospheric infrared emissions near 4.3 μm as output. These predictions then may be compared against the infrared measurements in order to judge the accuracy of the theory in predicting nuclear enhanced emissions as the result of nuclear energy deposit in the upper atmosphere.

Details of the spatial, spectral and temporal dependence of the nuclear enhanced infrared are all of prime importance for the effective design and/or performance evaluation of military optical systems which are supposed to be able to function in the presence of a nuclear enhanced background. Therefore, the auroral measurements program must be designed to obtain the temporal and

spatial dependence of both the energy deposit, and of the resultant enhanced infrared, in as great a detail as possible. Likewise, the ultimate theoretical capability we hope to develop, a capability to predict the infrared enhancements which result from the energy deposit, must be very detailed in order to accurately predict the detailed spatial, temporal and spectral distribution of enhanced 4.3 μm radiation as the result of a given time history of the spatial distribution of upper atmospheric nuclear (or auroral) energy deposit. Our tasks under this current contract are aimed at developing a portion of this theoretical capability. These tasks are concerned with evaluation of rocket measured 4.3 μm auroral zenith radiance data obtained in the DNA/AFGL auroral measurements program. One of these tasks was to develop facility to numerically solve the exact time dependent plane parallel radiation transport equations which describe the CO_2 4.3 μm aurora and to use this facility to attempt to obtain closer theoretical agreement with 4.3 μm data obtained on the dates 24 March 1973 and 27 March 1973 than had been obtained in an earlier preliminary study (Reference 1, Kumer, AFCRL-TR-74-0334). The second task was to perform preliminary analyses of 4.3 μm zenith radiance data that were obtained on 25 February 1974, 11 April 1974 and in March 1975.

The highlights of our study are: (1) We successfully developed the numerical facility to solve the exact time dependent plane parallel radiation transport equations which describe 4.3 μm emission in the upper atmosphere. (2) Accurate modeling for high altitude CO_2 4.3 μm emissions requires that the effects of the weak CO_2 4.3 μm bands are included in the calculation. (3) The 4.3 μm data consistently exhibit evidence for a 4.3 μm airglow layer due to the process $OH(v) + N_2 \overset{VV}{\rightarrow} OH(v-1) + N_2^{\ddagger}$, $N_2^{\ddagger} + CO_2 \overset{VV}{\rightarrow} N_2 + CO_2(\nu_3)$, $CO_2(\nu_3) \rightarrow CO_2 + h\nu$ (4.3 μm). About 0.06 to 0.22 ergs/cm^2 sec $N_2^{\ddagger}$ excitation is required. (4) A facility to use the ground based photometric data on the history of auroral emissions at 6300 Å (red) and at 4278 Å (or 3914 Å, blue) in order to generate the time history of the altitude dependence of energy deposit $q(z,t)$ by particle precipitation was developed and successfully applied for analysis of auroral 4.3 μm data obtained 25 February 1974. (5) The data obtained in 2 rocket flights 6 March 1975 under conditions of a sunlit and dark atmosphere

respectively were consistently explained on the basis of our CO_2 4.3 μm airglow theories of scattering and flourescence of sunlight by CO_2 in the sunlit case, and the $OH^{\ddagger}$ driven CO_2 4.3 μm nightglow in the dark case.

Further work to improve our modeling capability for 4.3 μm auroral data should include:

1) Development of a facility to calculate the spectral structure of the 4.3 μm zenith radiance. This requires calculating the altitude profiles of the radiance in each of approximately 400 lines in the CO_2 bands near 4.3 μm. Predictions of 4.3 μm spectral structure obtained in this way may be validated and improved on by comparisons with the spectral zenith radiance data obtained in the HIRIS flight of 1 April 1976, as well as by comparison with available short wavelength CVF spectrometer data.

2) Development of a capability to calculate the lateral structure in the 4.3 μm radiance as the result of lateral structure in the energy deposit by the high latitude mechanisms.

3) Apply our newly developed facility to generate q(z,t) from ground based red and blue photometric data (BRIM) for the further evaluation of data obtained 9 March 1972, 24 March 1973 and 27 March 1973. This effort should result in a more consistent picture for the interpretation of all of the 4.3 μm data obtained to date. In particular it should result in considerably narrowing the broad range for ϵ, the efficiency for producing $N_2^{\ddagger}$ from particle precipitation. Current bounds are $3 \leq \epsilon \leq 16$ (N_2 Vibration quanta/ionization event).

4) Study the correlation between ground based OH airglow data and the features in the 4.3 μm zenith radiance data which may be due to vibration transfer from $OH^{\ddagger}$ to N_2.

Performance of these tasks will commensurately improve our capability for accurate prediction of nuclear enhanced 4.3 μm atmospheric emission.

2.0 IMPROVEMENTS IN THE CO_2 4.3 μm AURORAL MODEL

2.1 Introduction

Preliminary evaluation of 4.3 μm zenith radiance data obtained on one rocket flight during 1972 and on two more during 1973 as part of the DNA/AFCRL ICE CAP infrared auroral measurements program (Stair et al., Reference 2, 1975) has been given in summary form by Kumer, Reference 3, 1975, and in more detail by Kumer, Reference 1 (henceforth References 3 and 1 will be referred to by KSP and CRLO334, respectively). In these preliminary evaluations it was shown that the dominant mechanism for producing the observed data is vibrational excitation of nitrogen by precipitating electrons followed by VV exchange with CO_2 to form CO_2 (001) followed by radiation in the CO_2 ν_3 fundamental band 001 → 000 near 4.3 μm. The basic processes involved in this $N_2^{\ddagger} \rightleftharpoons CO_2$ (001) mechanism are reactions (1) through (6) in KSP. The basic time dependent radiative transfer equations which describe the $N_2^{\ddagger} \rightleftharpoons CO_2$ (001) mechanism are (7) and (8) in KSP. A stationary time dependent approximation (STDA) for solving these equations is developed in the KSP and CRLO334 papers. It is shown in these papers that plausible agreement between theory and data is achieved via this approach.

In our present report we show that the inclusion in equations (7) and (8) of KSP of a term which accounts for 4.3 μm radiation to space by CO_2 ν_3 bands other than the $^{12}C^{16}O_2$ fundamental 001 → 000 band is an important mechanism for determining the $N_2^{\ddagger}$ lifetime τ in the altitude range $65 \leq z \leq 90$ km, and that in fact an error of a factor 3 excess in τ at $z \cong 75$ km will be made if this mechanism is neglected. We also describe an exact time dependent transport (TDT) method for solving the corrected versions of equations (7) and (8) of KSP. We show that solution of these equations via this more accurate method provides a better fit to the data obtained 24 March 1973 than we had previously reported (CRLO334). We also show that reasonable agreement with data obtained 6 March 1975 in the twilight sunlit atmosphere may be achieved via application of the TDT method.

2.2 The Weak CO_2 ν_3 Bands

In the meteorological community it has been known for some time that weak CO_2 bands near 15 μm play an important role in the mesospheric heat budget. (See Reference 4 for example.) This would suggest that weak CO_2 ν_3 bands might play an important role in the $N_2^{\pm} \rightarrow CO_2$ (001) aurora. Indeed, in our earlier report (CRL0334, Appendix C) we introduced an approximate method for including the contribution of the weak CO_2 ν_3 bands to the CO_2 ν_3 4.3 μm zenith radiance. We showed that the weak band contribution to CO_2 ν_3 zenith radiance was indeed a major effect. In that report (CRL0334) we did not however consider what effects the weak ν_3 bands would have on the time dependent radiative transport of CO_2 ν_3 photons.

In our current work we do consider the transport effect of these weak CO_2 ν_3 bands, and we show that these effects are significant. The weak CO_2 ν_3 bands we include in our calculation are shown in Table 1. These bands form a nearly complete set in that addition of weaker bands does not significantly impact the problem in the altitude region of interest. The CO_2 isotope notation follows McClatchey *et al*. (Reference 5). The bands are designated by the number j.

2.3 The Time Dependent Radiative Transfer Equations

If we treat the upper state populations $[CO_2 (j\nu_3)]$ of each weak CO_2 ν_3 band in Table 1 as an unknown, as well as $[CO_2 (001)]$ and $[N_2^{\pm}]$ as unknowns, we get 12 unknown quantities at each altitude mesh point (the role of the altitude mesh points in computing the radiative transfer integral is discussed by Kumer and James, Reference 6, this paper will be henceforth referred to by KJ). These quantities are coupled with each other due to VV transfer between N_2 and CO_2, and they are coupled to the quantities at all other altitudes due to radiation transport. Currently we use an altitude mesh consisting of 26 points. Hence, the exact description of the problem involves the solution of 12 x 26 coupled time dependent integral radiation transport equations that are similar to equations (7) and (8) in KSP.

Table 1. THE WEAK CO_2 ν_3 BANDS

j	$CO_2(j\nu_3) \rightarrow (j)$ Transition	Isotope
2	$00^0 1 \rightarrow 00^0 0$	636
3	$00^0 1 \rightarrow 00^0 0$	628
4	$00^0 1 \rightarrow 00^0 0$	627
5	$01^1 1 \rightarrow 01^1 0$	626
6	$01^1 1 \rightarrow 01^1 0$	636
7	$01^1 1 \rightarrow 01^1 0$	628
8	$01^1 1 \rightarrow 01^1 0$	627
9	$02^2 1 \rightarrow 02^2 0$	626
10	$02^0 1 \rightarrow 02^0 0$	626
11	$10^0 1 \rightarrow 10^0 0$	626

We define $f_j = [\nu_3 j]/[j]$ and $f_N = [N_2^{\ddagger}]/[N_2]$. Here $[\nu_3 j]$ is the population of the upper state of the jth ν_3 band, and $[j] = G_j[CO_2\ (000)]$ is the population of the ground state of the jth ν_3 band. The G_j are the relative number densities of the ground state CO_2 for bands j as compared to the major isotopic CO_2 626 specie 001 → 000 ground state number density $[CO_2\ (000)]$. The G_j for the 001 → 000 band of the minor isotopic specie are well known. The calculation of G_j for the hot bands of all the isotopic species requires that the CO_2 ν_2 vibrational temperatures T_{ν_2} are known. Our method for calculating the T_{ν_2} is given in a paper (Reference 7, "CO_2 and N_2 Vibrational Temperatures, 40 to 140 km") that we have submitted for publication (1976) to J. Geophys. Res.

The homogeneous equations analogous to (7) and (8) in KSP are

$$\frac{d}{dt} f_j = k_2[N_2][(f_N - f_j) - k_1[M] f_j - A_L f_j$$

$$- A_{4.26}\left\{E_j f_j - \int \sigma\, w_j^{-1}\, G_j' dN_j' H_{bP}\left(\sigma\, w_j (N_j - N_j')\right)\left(f_j(N') - f_j(N)\right)\right\} \qquad (1a)$$

and

$$\frac{d}{dt} f_N = k_2'[CO_2]\, \Sigma G_j (f_j - f_n) - (k_{10}[O] + k_{ell}[O_2]) f_N \quad . \qquad (1b)$$

The quantities N_j are defined by

$$N_j = \int_j^{\infty} dZ'\, G_j(Z')\, [CO_2\ (000)] \quad .$$

The quantities w_j are 1 or 1/2 depending on the symmetry properties of the jth band, $w_j = 1$ for j = 1, 10 and 11, and $w_j = 1/2$ for all other j. The quantities E_j are the escape functions for the jth band, and

$$E_j = E_{bP}(w_j \sigma N_j) + E_{bP}[w_j \sigma (N_{jL} - N_j)]$$

where $N_{jL} = N_j(z_L)$ and z_L is the lower boundary, $z_L = 40$ or sometimes 50 km for the results we will present in Section 3.0 of this report.

The quantities A_L account for fluorescent radiation near 9.6 and 10.4 μm from all of the upper levels $[\nu_3 j]$. There is an additional contribution of about 4% of $A_{4,26}$ to the A_L for values of j = 10 and 11. The extra contribution to A_L for the j = 10 and 11 bands is due to the 2.7 μm transitions $02^0 1 \rightarrow 00^0 0$ and $10^0 1 \rightarrow 00^0 0$ (James and Kumer, Reference 8, 1973).

Other quantities appearing in equations (1) are defined in KJ. Also quantities which appear subsequently herein, and which are not defined herein, are in fact defined in either KJ or CRL0334. Values for the rate constants that we use for the calculation reported herein have been modified from what is listed in KJ, when necessary, in order to conform with the latest values reported by Taylor, References 9 and 10.

2.4 Escape Function Approximations for the $N_2^{\pm}$ Relaxation Time

The 12 x 26 coupled equations (1) are numerically too difficult to conveniently solve with computing facilities available to us. It is possible however to use the escape function approximation (see KSP and/or CRL0334) to estimate the relaxation time $\tau(z)$ for an $N_2^{\pm}$ created at an altitude z. The escape function approximation (EFA) is implemented by setting the integral term to zero in equation (1b). The 12 x 26 coupled equations (1) reduce to 26 sets of 12 x 12 equations, each set associated with a specific z mesh point. Each of the sets of 12 coupled equations are linear first order differential equations, just like equations (1). Formally the inhomogeneous matrix form of the equations may be written

$$(I \frac{d}{dt} + U) f = \eta \qquad (2)$$

where I is the unit matrix, elements of U may be determined from the homogeneous equations (1) and η is an inhomogeneous vector term. If one knows the eigenvector matrix K such that $UK = K\lambda$ where λ is a diagonal matrix of eigenvalues, and if one knows K^{-1} such that $K^{-1}K = I$, then the operation

$$K^{-1}(I \frac{d}{dt} + U) K K^{-1} f = K^{-1} \eta \qquad (3)$$

yields the diagonalized set of equations

$$\left(I\frac{d}{dt}+\lambda\right)f' = \eta' \tag{4}$$

where $f' = K^{-1}f$ and $\eta' = K^{-1}\eta$. The solution of (2) then is Kf' where

$$f' = \int_{-\infty}^{t} dt' \, e^{-\lambda(t-t')} \, \eta'(t') \tag{5}$$

For each of the 26 sets of 12 x 12 equations obtained from equations (1) by EFA there are 26 sets of 12 eigenvalues λ. These eigenvalues are inverse time constants associated with the eigenvectors in the K matrix. In each set λ there is one small inverse time constant λ_N and 11 large inverse time constants λ_j.

The quantity $\tau_N = 1/\lambda_N$ gives the decay time of the initial $N_2^{\ddagger}$. The short lived time constants $\tau_J = 1/\lambda_j$ correspond roughly to the rapid decay of the initial $[\nu_j]$ due to radiation to space.

The K, λ and K^{-1} may be readily attained numerically by using standard scientific computer subroutines. The LMSC adaptation of the CACM algorithm 343 12-68(820), EIGENP may be used to obtain the K and λ associated with U. Next, the widely used subroutine GJR may be used to obtain K^{-1}. If necessary, double precision results may be obtained by using EIGEND and DGJR.

2.5 The Q_w Approximation

The 12 x 26 coupled equations (1) may be reduced to 2 x 26 coupled equations if one introduces a term Q_w which approximates the effects of the weak bands in quenching $N_2^{\ddagger}$. We define

$$Q_w \equiv k_2'[CO_2] \sum_{j=2}^{11} G_j \left(\frac{A_{4.26}E_j + A_L + k_1[M]}{A_{4.26}E_j + A_L + k_1[M] + k_2[N_2]} \right) .$$

The Q_w approximation for equations (1) is

$$\frac{d}{dt} f_1 = k_2[N_2](f_N - f_1) - (k_1[M] + A_L) f_1$$
$$- A_{4.26} \left\{ E_1 f_1 - \int \sigma \, dN_1' H_{bP}(\sigma | N_1 - N_1' |) (f_1' - f_1) \right\} + \eta_1 \qquad (6a)$$

and

$$\frac{d}{dt} f_N = k_2'[CO_2] (f_1 - f_N) - (k_{10}[O] + k_{e11}[O_2] + Q_w) f_N + \eta_{NQ_w} \quad . \qquad (6b)$$

The 2 x 26 coupled equations (6) are of the form of equation (2) and may readily be solved numerically by the techniques described in Section 2.4 on the computing facilities that are available to us. We will designate such a "time dependent transport" solution by TDT,Q_w for solution of equations (6). In reference to solution of equations (1) we shall use *TDT*.

In the Q_w approximation we use a *modification* for η_N defined by

$$\eta_{NQ_w} = \eta_N + \sum_{j=2}^{11} \frac{G_J [CO_2]}{[N_2]} \eta_j F_{Nj}$$

and

$$F_{Nj} \equiv \frac{k_2[N_2]}{k_2[N_2] + k_1[M] + A_L + A_{4.26} E_j} \quad .$$

This *modification* accounts for the VV transfer $CO_2 (j\nu_3) \rightarrow N_2^{\ddagger}$ of initial excitation in band j over to $N_2^{\ddagger}$. This "weak band related pumping" process for $N_2^{\ddagger}$ is the opposite process of the "weak band related quenching" process which we account for by the psuedo-quenching term Q_w in equations (6).

The TDT,Q_w approximation for f_j for $j \geq 2$ may be obtained by setting $\frac{d}{dt} f_j = 0$. This approximation is useful if $|\frac{d}{dt} \eta_j| \ll \lambda_N |\eta_j|$. The result is

$$f_j \simeq (k_2[N_2] f_N + \eta_j) / (k_2[N_2] + k_1[M] + A_L + A_{4.26} E_j) \qquad (7)$$

2.6 Accuracy of th Q_w Approximation

We must address the question of the accuracy of the Q_w approximation. We obtained no TDT solutions of equations (1) for comparison with TDT, Q_w solutions of equations (6), but we were able to obtain EFA solutions of equations (1) which may then be compared with EFA solutions of equations (6). In EFA equations (6) reduce to 26 sets of coupled 2 x 2 equations with two associated eigenvalues of which λ_N is the smaller, $\tau = 1/\lambda_N$. The estimated $N_2^{\ddagger}$ relaxation time constants $\tau = 1/\lambda_N$ obtained from these EFA calculations are shown in Figure 1. The curve labeled EFA, Q_w applies for the EFA solution of equations (6) with Q_w given by equation (5). The curve labeled EFA, $Q_w = 0$ applies for EFA solution of equations (6) with $Q_w = 0$. The curve labeled τ_{PI} is given by $\tau_{PI} = (k_2'[CO_2] + k_{10}[O])^{-1}$, this value for τ_{PI} assumes no back VV transfer from CO_2 $(j\nu_3)$ to N_2.

The EFA, $Q_w = 0$ estimate for τ is incorrect since it neglects the transport effect of the weak bands. The EFA, $Q_w = 0$ estimate for τ was reported in KSP and CRL0334 since the transport effects of the weak bands had not as yet been considered at the time those documents were published. Since the 3 estimates are quite similar for $z \gtrsim 90$ km, and since the bulk of the auroral energy deposition occurs for $z \gtrsim 90$ km, the 4.3 μm auroral zenith radiance data analysis and the conclusions presented in the papers KSP and CRL0334 are essentially correct. However, we shall see below that analysis of the auroral data via TDT, Q_w solutions does achieve a somewhat better match of the data with theory than that which is shown in KSP or CRL0334.

The EFA, $Q_w = 0$ estimate for τ becomes much different than the other two estimates for altitudes $z \lesssim 90$ km. This is a very important point of interest for DNA because the bulk of the energy deposit from high altitude detonations occurs for $z < 90$ km. We believe some kind of rocket experiment to confirm the effect of the weak bands on τ in region $z < 90$ km is necessary. Sunrise or sunset twilight shots might be useful for this purpose. However in Section 3.5 below we show that in the case of the existing 6 March 1975 twilight sunlit data that the η_1 and $\eta_{N_{Qw}}$ are changing rather slowly over a time scale $\tau(z)$

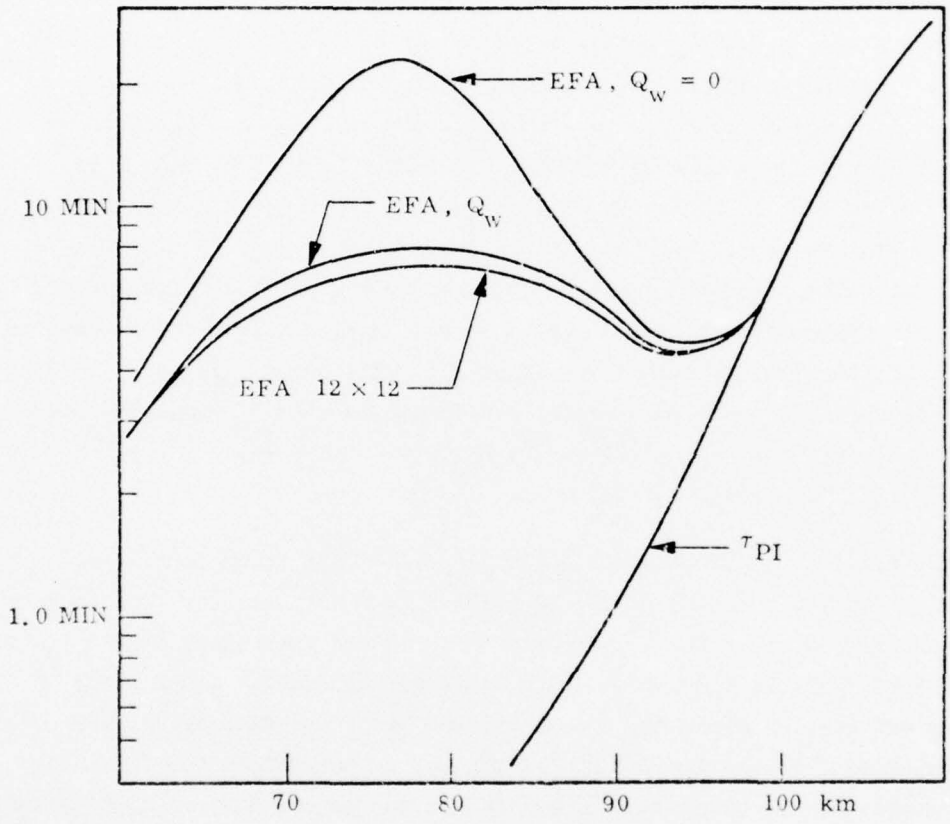

Figure 1. A comparison of the EFA estimates for the $N_2^{\ddagger}$ relaxation time τ. The curves labeled EFA, Q_W and EFA 12 x 12 include the effects of the weak CO_2 ν_3 bands, the curve labeled EFA, $Q_W = 0$ does not. The curve labeled τ_{PI} is the result one achieves by neglecting the vv transfer from CO_2 back to N_2.

and therefore the time dependent effects are mild enough that they are not dramatically evident in these data.

A second important point that Figure 1 illustrates is that the EFA 12 x 12 and the EFA, Q_w estimates for τ are virtually identical. This means that the Q_w approximation of equations (6) to equations (1) is very accurate for the purpose of computing the $N_2^{\pm}$ relaxation time.

In Section 3.1 below we will examine the impact of using the more accurate τ estimate (by EFA 12 x 12 or EFA, Q_w) as compared to using the less accurate τ estimate EFA, $Q_w = 0$ for the analysis of 4.3 μm zenith radiance altitude profile data obtained by Stair et al. (Reference 2) in a rocket experiment on 27 March 1973. In Section 3.1 we will refer to these two estimates as τ_c and τ_f respectively.

In a paper recently submitted to Journal of Geophysical Research (Reference 11, Kumer, "Theory of the CO_2 4.3 μm Aurora and Related Phenomena," 1976) we compare in detail the approximate calculation of quiet night time zenith radiance profiles and of auroral zenith radiances by EFA, Q_w and by EFA 12 x 12. We find that the radiances calculated by these 2 methods are essentially identical, just as τ_c calculated by the 2 methods is essentially identical (see Figure 1). We concluded then that radiances calculated by the TDT and TDT, Q_w would also be essentially identical. Thus in the remainder of this paper we shall designate radiances calculated by TDT, Q_w simply as radiances calculated by TDT.

The reader should bear in mind that radiance calculations by TDT are intrinsically more accurate than calculations by EFA since in the later case vertical radiative photon diffusion is neglected. The EFA, Q_w and EFA 12 x 12 radiance calculations that we discuss in Reference 11 were generated for the sole purpose of establishing that the TDT, Q_w and TDT radiance calculations should be essentially identical.

2.7 Radiances in the Weak Bands

In Section 2.6 above we showed that neglect of the weak CO_2 ν_3 bands results in a large error in the computed $N_2^{\ddagger}$ relaxation time $\tau(z)$ in the altitude region $z < 90$ km. Here in Section 2.7 we will show some calculational results to illustrate that large errors in the computed radiance profiles will also occur at lower altitudes if the weak bands are neglected.

We show the 4.3 μm zenith radiance profiles calculated by TDT in selected bands in Figures 2 and 3. Profiles in Figure 2 are calculated for the ambient night time (March 65°N model atmosphere) case. Profiles in Figure 3 are calculated for the 24 March 1975 $\epsilon q(z,t)$ auroral deposition model $\epsilon q(z,t)$ that we used in our previous study (KSP and CRL0334). The inhomogeneous terms η_N and η_j appropriate for the auroral case are

$$\eta_N(z_i,t) = \epsilon q(z_i,t)/[N_2]_{z_i}$$

and

$$\eta_j(z_i,t) = 0 \quad .$$

The inhomogeneous terms η_j for the ambient night time calculation are given by

$$\eta_j = 4\sqrt{\pi}\, R\lambda_D E_{bP}[(N_{jL}-N_j)\sigma] + k_1'[M] \quad . \qquad (8a)$$

The first term on the right hand side (RHS) of equation (8a) η_{jes} accounts for absorption of earthshine emitted from altitude z_L (see KJ, page 645), the 2nd term on the RHS of equation (8a) η_{jc} accounts for thermal collisional excitation from $CO_2(j\nu_3)+M \rightleftharpoons CO_2(j\nu_1\nu_2)+M$. Since $k_2[N_2] \gg \eta_{jc}$ for all altitudes no accuracy is lost by making the approximation $\eta_{jc} = \eta_{1c}$. The calculation of η_{1c} is discussed more thoroughly in our paper (Reference 7).

Collisional excitation of $N_2^{\ddagger}$ is responsible for the ambient night time value for $\eta_N(z_i)$ which are given by (see KJ, pages 640 and 641)
$\eta_N = E_{N_2}/[N_2]$.

For the ambient night time calculation we take $d/dt\ \eta_j = 0 = d/dt\ \eta_N$.

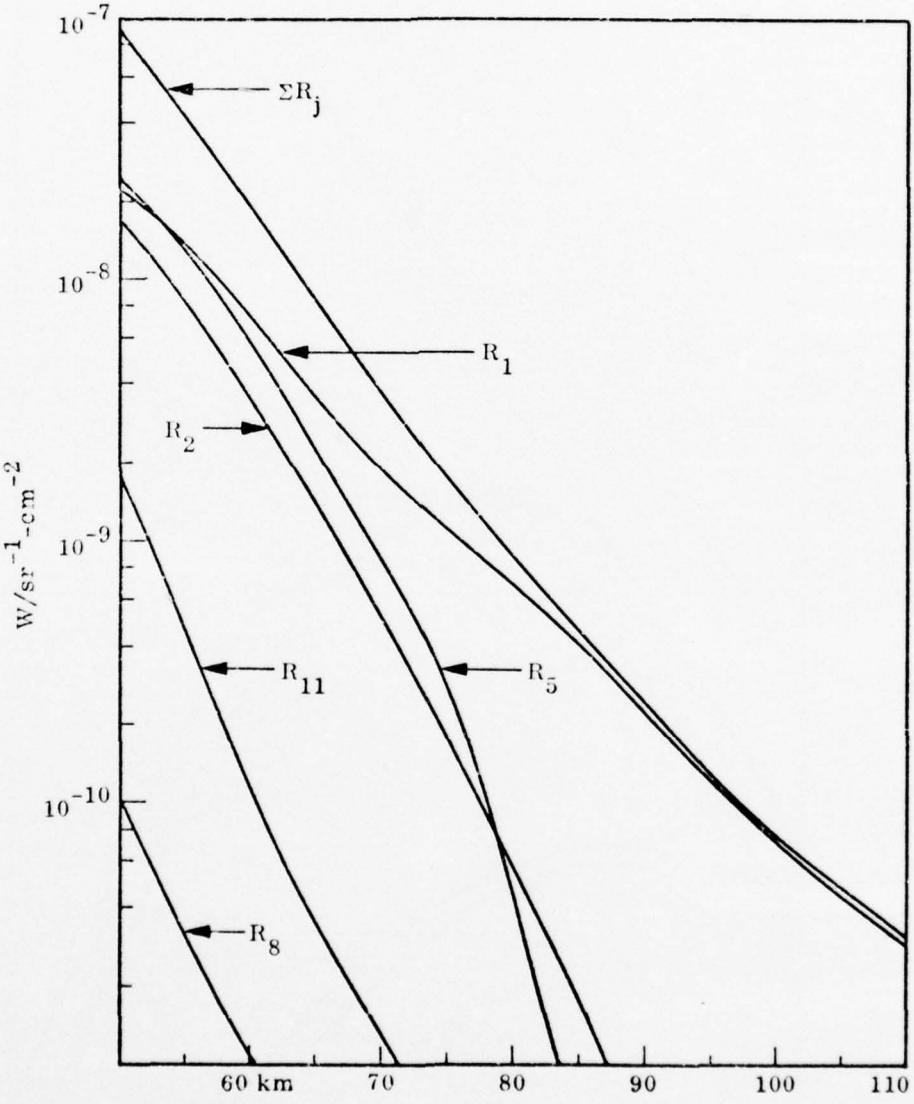

Figure 2. Ambient night time 4.3 μm radiance profiles calculated by TDT for the total 4.3 μm radiance ΣR_j and in selected bands R_j (j = 1,2,5,8 and 11).

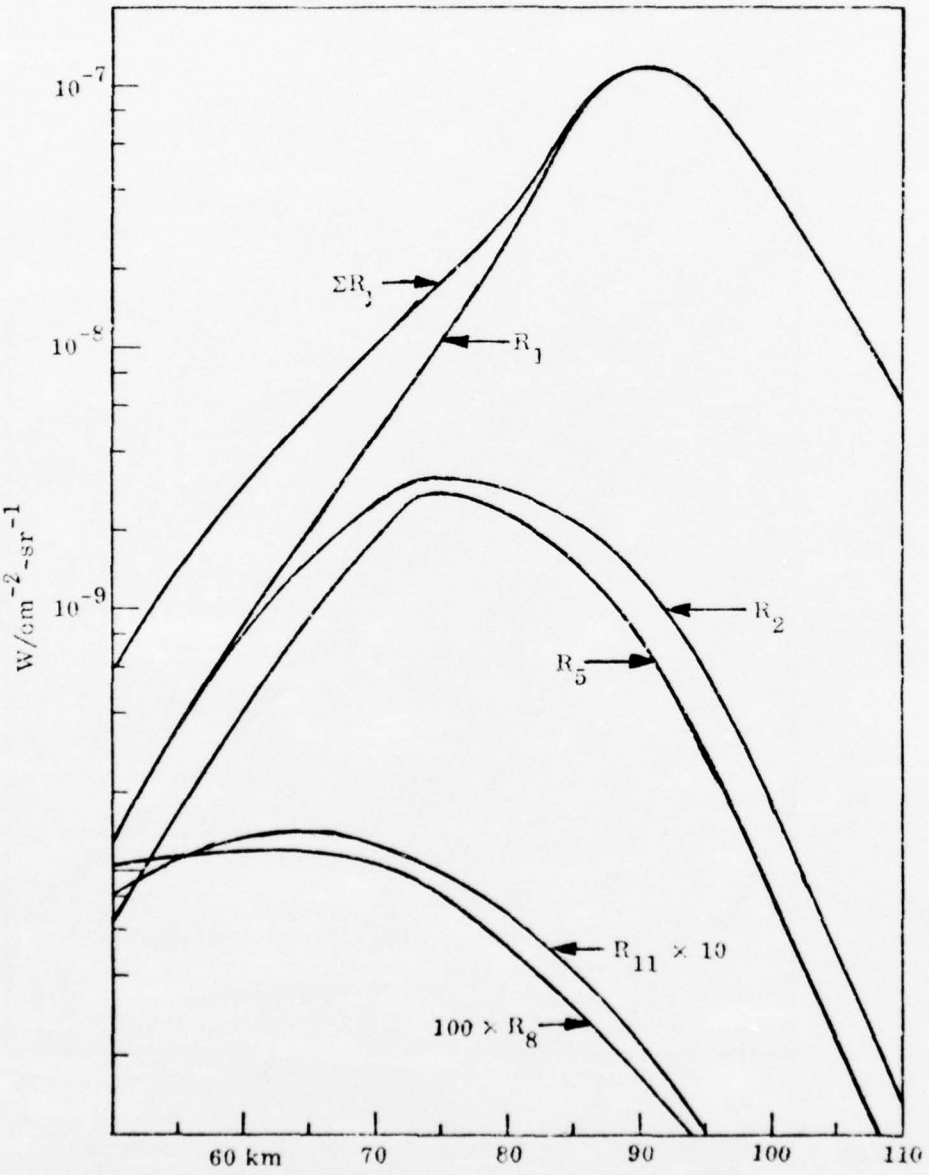

Figure 3. Auroral radiance profiles calculated by TDT for the 24 March 1973 deposition model $\varepsilon q(z,t)$ are shown, these are $\sum_{j=1}^{11} R_j$ and selected R_j (j=1,2,5,8 and 11).

Considering that $\tau \leq 20$ min in the altitude region of interest, this is an accurate representation for the time dependence of η several hours after sunset.

Using these two sets of values for η, one set appropriate for the 24 March 1973 aurora, the other set appropriate for quiet night time conditions, we may solve equations (6) to obtain two corresponding solution sets f_j. From the f_j the radiance R_j in a given band may be computed via

$$4\pi R_j = \int \sigma \, dN_j' T_b(\sigma w_j |N_j' - N_j|) \Omega_j(N_j') S_j(N_j') \qquad (8b)$$

where

$$\Omega_j S_j = \sigma^{-1} A_{4.26} f_j \quad .$$

Radiance profiles for the sum ΣR_j of the radiance in all bands, for radiance in the 626 fundamental R_1, for radiance in the strongest minor isotopic band R_2, for radiance in the strongest major isotopic hot band R_5, for radiance in the weakest major isotopic hot band R_{11}, and for radiance in the weakest minor isotopic hot band R_8 are shown on Figures 2 and 3. By inspecting these results we see that the stronger weak bands R_2 and R_5 are very significant for $z \leq 80$ km. Indeed neglecting R_2 and R_5 would lead to gross inaccuracy for $z \leq 70$ km. On the other hand since the weaker of the weak bands, R_8 and R_{11}, are insignificant for $z \geq 50$ km, we believe that the set of bands shown in Table 1 is complete for the purpose of calculating the CO_2 ν_3 4.3 μm radiance which originates from $z \geq 50$ km. Thus we illustrate that the weak bands contribute very significantly for altitudes $z \leq 80$ km.

3.0 DATA EVALUATION

3.1 Applications of Data Obtained 24 March 1973

We use the model $\epsilon q(z,t)$ which is described in KSP and CRL0334 for the 24 March 1973 aurora for both the up and downlegs, and we use TDT to calculate ΣR_j for comparison with the auroral 4.3 μm zenith radiance altitude profile data (Reference 2). These calculations and the data are shown in Figure 4. Less recent calculations taken from KSP and CRL0334 are also shown. As expected there is little difference in the older and newer calculations above 90 km.

The weak bands become important for loss of vibrational quanta by radiation to space near $z \simeq 80$ km, this manifests itself by the markedly better fit to the upleg data which is achieved with the newer calculations in this altitude region.

The fit to the downleg appears equally good in each case. The downleg deposition model for $\epsilon q(z,t)$ is probably less certain than is the upleg model however, and the quality of the theoretical fit can be no better than the input model. In fact we can imagine the use of a somewhat inaccurate deposition model which would yield a better fit to the data on input to a somewhat inaccurate theoretical calculation, than might be obtained on input to a very accurate theoretical calculation, provided that the inaccuracies in the former case are accidentally compensatory.

More information on deposition models for 24 March 1973 have recently become available. This information appears in various publications including for example References 12, 13 and 14. In addition to the energy input modeling for 24 March 1973 which has been performed at other institutions, in our current effort we have developed a capability to generate a spatial and temporal energy input model $q(z,t)$ from ground based photometric observations of the histories of the auroral 6300 Å and 4278 Å (or 3914 Å) emissions. We call this capability BRIM (blue red input model). It would be a useful and rather inexpensive exercise for us to utilize the input model information for the 24 March 1973 event which has been published by other authors, and to also

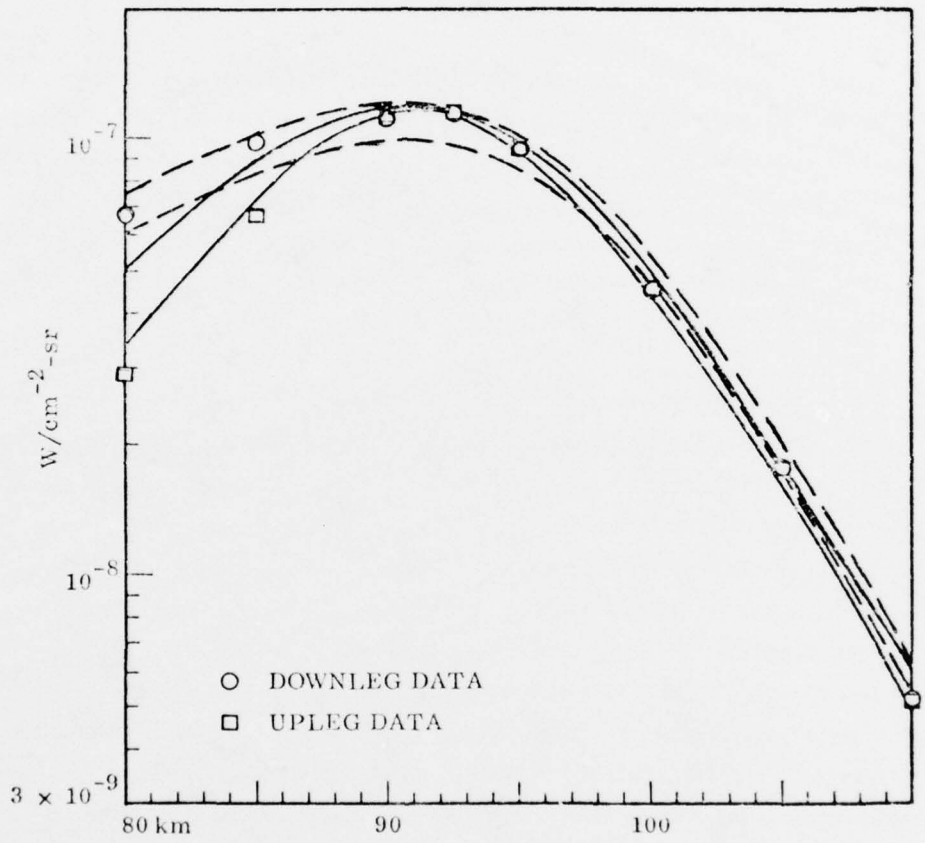

Figure 4. The 24 March 1973 4.3 μm auroral zenith radiance data (Reference 2) are compared with predictions. The solid curves are TTD predictions. The dashed curves are the older STDA predictions (KSP and CR0334). Up and downleg predictions are labeled by U and D. The ε values in units (N_2^+ per ion pair) which provide the best fit are:

TTD		STDA	
U	D	U	D
14.9	13.9	16.3	14.5

utilize our BRIM capability in application to ground based photometric data obtained on 24 March 1973 in order to devise a model for $q(z,t)$ for 24 March 1973 which is more carefully constructed than the older, preliminary model we describe in KSP and CRLO334. We could then compare the 4.3 μm zenith radiance profiles we calculate on the basis of the improved input model with the data. The purpose of the exercise would be to develop more credibility in our TDT calculation, and to quantitatively establish what is the contribution as the result of uncertainty in the energy input model to uncertainty in the value for ϵ extracted from the 24 March 1973 data.

3.2 Implications for Evaluation of Data Obtained 27 March 1973

The mildly varying altitude dependence of what we currently believe to be the N_2^+ relaxation time τ_c in the 70 to 100 km region has some important and interesting consequences for the interpretation of downleg 4.3 μm zenith radiance data obtained 27 March 1973 (CRLO334). These data are shown in Figure 5 compared against a radiance profile labeled M2. This profile is our non LTE prediction for the ambient night time 4.3 μm zenith radiance. The model atmosphere for the M2 calculation is based as much as possible on independent measurements of the atmospheric temperature. Development of the M2 model atmosphere is described in detail by Kumer (Reference 15). The downleg penetration occurred at a location where the only deposition, at the time of penetration and indeed for at least 45 min prior to penetration, was a soft precipitation which produced about 1.5 kR of 3914 Å brightness, most of this above 115 km where the N_2^+ is predominantly quenched by O rather than CO_2. In CRLO334 it is shown that this drizzle could not be responsible for the "flattening" or "maximum" which is noted in the data in the 70 to 80 km altitude region.

Since our former calculation (CRLO334) for τ_f the N_2^+ relaxation time (calculated via EFA, $Q_w = 0$) has a prominent maximum of more than 20 min near 75 km we had once thought (CRLO334) that this maximum in the 27 March 1973 downleg 4.3 μm zenith radiance data near 75 km might be the decaying remnant of a very bright aurora for which energy input may have terminated as long as

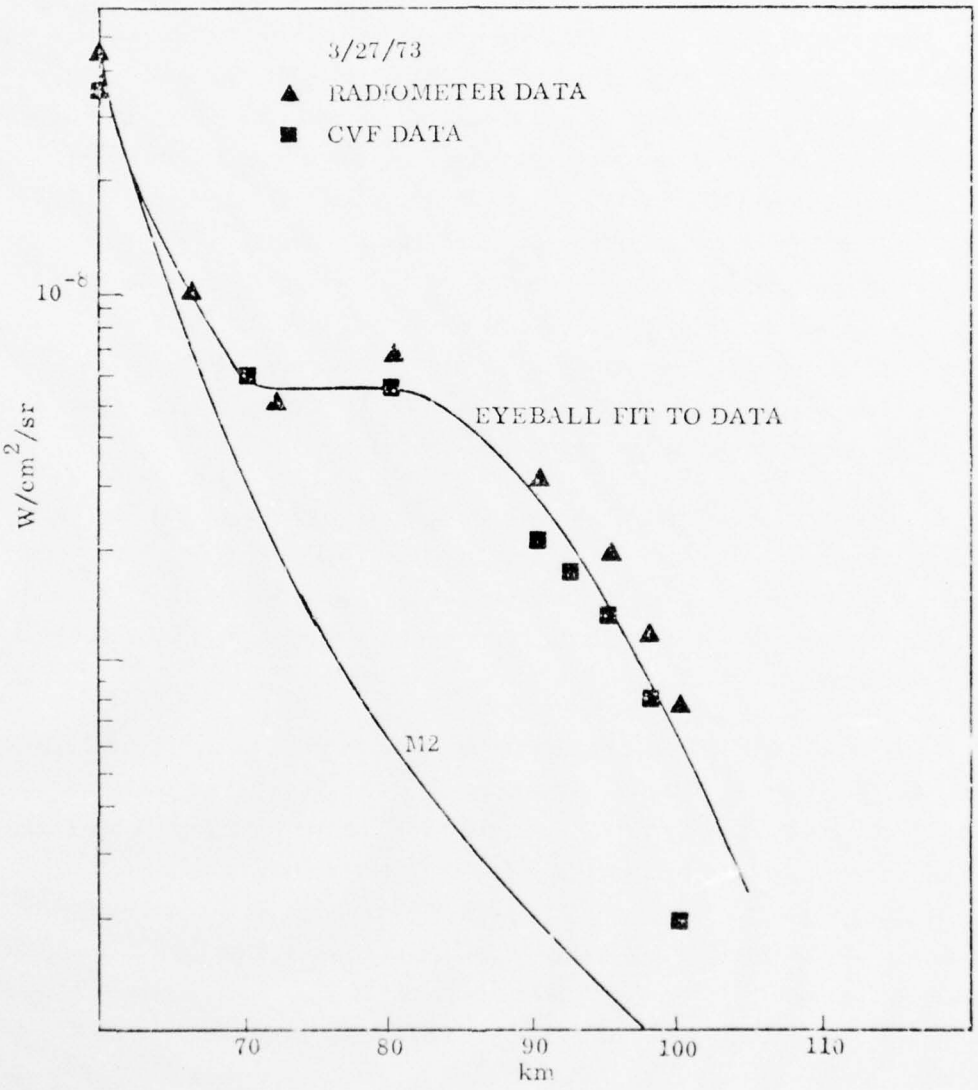

Figure 5. Auroral 4.3 μm zenith radiance data obtained on the downleg of a rocket experiment (Stair et al., Reference 2) conducted on 27 March 1973 are compared with an ambient night time radiance calculation (curve M2). The model atmosphere on which the ambient calculation is based is described by Kumer (Reference 15).

an hour or more prior to downleg penetration. We had made the assumption that there was no appreciable wind shear in the 70 to 95 km region. We had thought that the shift in position to lower altitude of the maximum in auroral 4.3 μm radiance would occur since the altitude dependence of τ_r dictates that the radiance profile of an intense aurora decays 4 times faster at 95 km than at 75 km after cessation of the energy input. The input is assumed to peak at about 95 km for "hard" auroral precipitations. However, since τ_c (our current, more accurate, calculation for the $N_2^{\ddagger}$ relaxation time) changes at most by a factor 1.7 in the altitude range $70 < z < 95$ km, this effect will not as readily occur. In fact the peak in the decaying auroral radiance profile should tend to shift from the 90 to 95 km region toward higher altitudes due to the rapid increase in τ_c above z = 95 km.

Thus we must look for alternate mechanisms to explain the "maximum" which occurs in the 27 March 1973 downleg data at about 75 km. The data requires that such a mechanism must produce a column source of N_2 excitation of about 0.2 ergs/cm^2 sec which is confined to a narrow layer which peaks near 80 km altitude.

We considered several candidate mechanisms such as (1) a hard particle flux, (2) $N + NO \rightarrow N_2^{\ddagger} + O$, (3) transport of $N_2^{\ddagger}$ by winds from distant auroras, and (4) the reaction $OH(v) + N_2 \rightarrow OH(v-1) + N_2^{\ddagger}$ which taps the OH airglow energy source. We now believe the OH mechanism is most likely responsible for the feature which occurs in the 27 March 1973 downleg data. We will elaborate on this point in Section 3.3 below where we discuss 4.3 μm zenith radiance data obtained on 11 April 1974 under quiet night time conditions. These data also show a feature near 80 km which is similar to that observed in the 27 March 1973 data. In fact, in the ensuing discussion we will show that similar evidence for an $OH^{\ddagger}$ driven CO_2 4.3 μm airglow also occurs in data obtained 6 March 1975, 25 February 1974 and probably also in the upleg data obtained 27 March 1973.

3.3 Evaluation of Data Obtained 11 April 1974

One of the ICE CAP 74 goals was to obtain a 4.3 μm zenith radiance profile under quiet conditions so that there would be no significant auroral component in the data thus obtained. The evening of 11 April 1974 was relatively free of auroral activity so the "quiet conditions" rocket was launched that evening. A preliminary version of the 4.3 μm zenith radiance data are shown on Figure 6. These data were provided by Ned Wheeler (Reference 16, private communication, 1976). A final version of these data will soon be published in a report (Reference 17) by Wheeler. In the preliminary data it appears that there is an altitude independent background of about 4.5 MR/μm which extends on up to apogee. The background is probably an artifact rather than atmospheric emission. This altitude independent background certainly is not due to ambient CO_2 emission. In order to get the quiet night CO_2 zenith radiance we are justified in subtracting the background 4.5 MR μm^{-1} from the data, no matter what the origin of the background. The result is labeled "data, background subtracted" on Figure 6.

We obtained ASL meteorological data (Reference 18) up to 60 km altitude for the evening of 11 April 1974. Above 60 km we joined this data smoothly to an April 65°N model G. V. Groves (Reference 19, AFCRL Report 70-0261) as shown in Figure 7. The temperature data shown on Figure 7 are necessary to calculate the non LTE ambient night time thermal 4.3 μm zenith radiance profile which is due to emission by CO_2.

The results of the non LTE thermal radiance calculations are compared with the background corrected data on Figure 8. Two calculations are shown. The one labeled "B" employs an approximation to attempt to account for the effects of the altitude varying temperature dependent change in band and line shape. This approximation involves multiplying the contribution to $S_o(No)$ from earthshine by a factor $B_R(T_L, T(z), N_L\text{-}N(z))$ where T_L is the temperature at z_L, $T(z)$ the atmospheric kinetic temperature at altitude z,

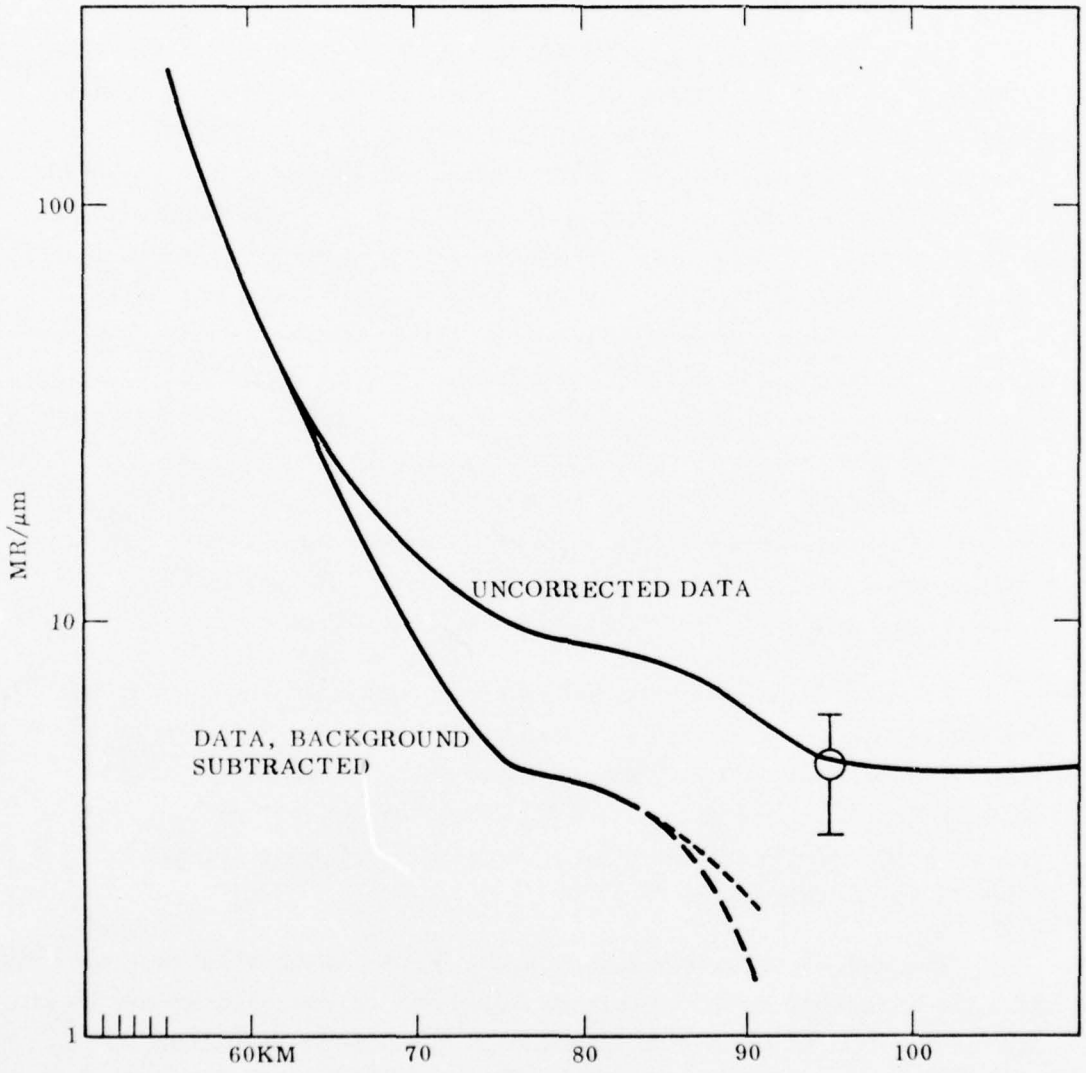

Figure 6. Preliminary version of 4.3 μm zenith radiance data obtained on 11 April 1974 under quiet conditions.

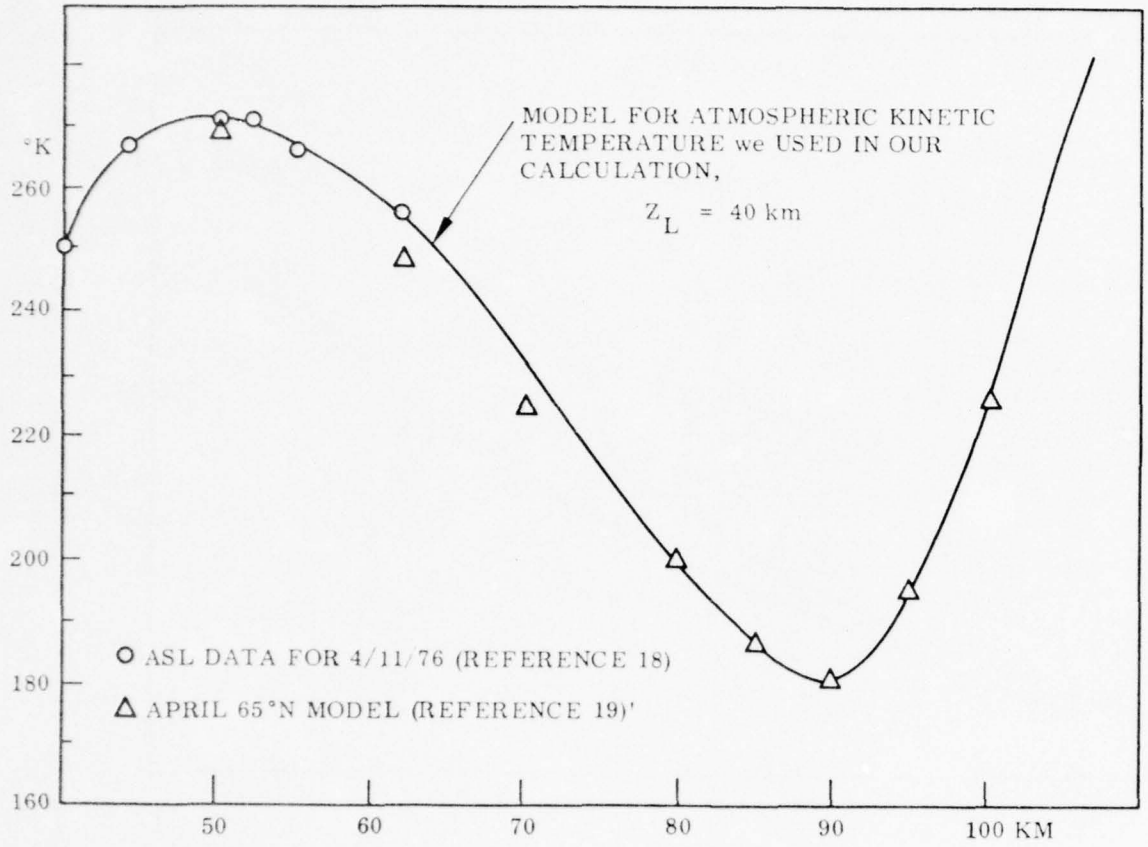

Figure 7. This figure illustrates our method for constructing a model temperature profile appropriate for 11 April 1974.

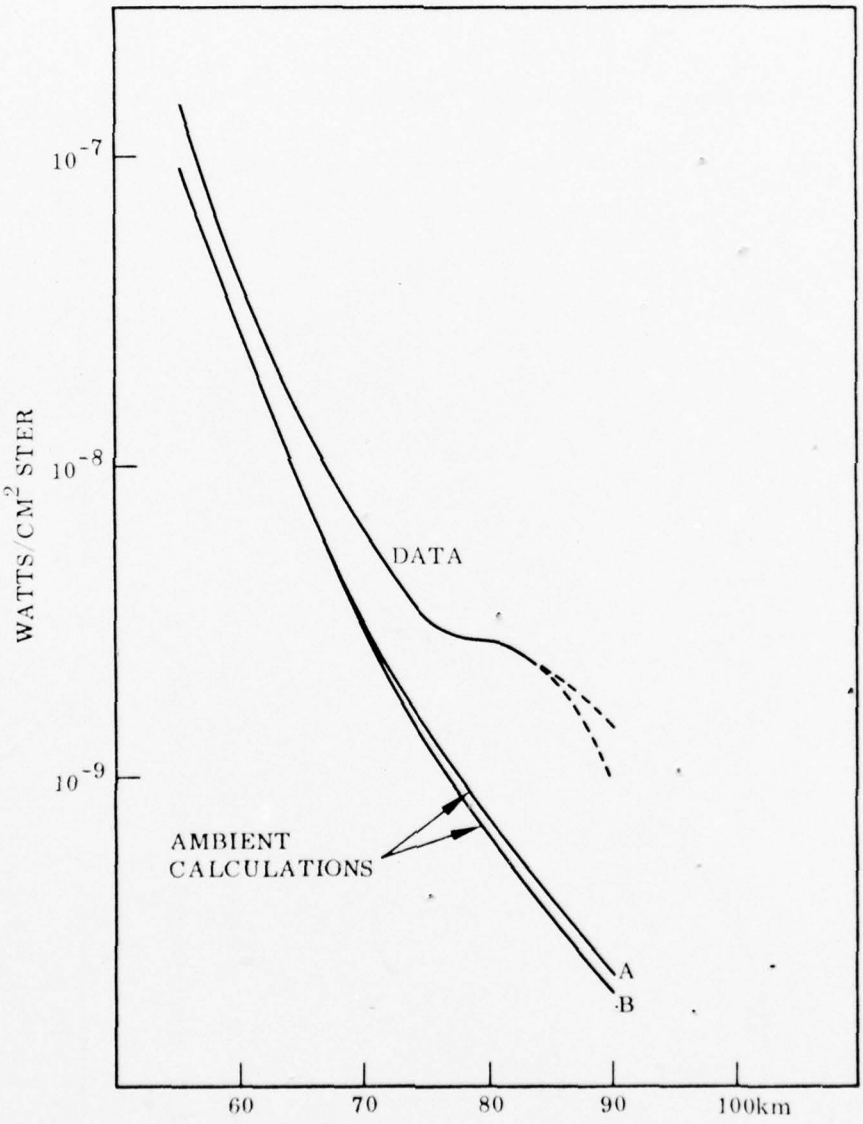

Figure 8. Ambient calculations are compared with the data.

$N(z) = \int_z^\infty dz[CO_2]$ and $N_L = N(z_L)$. The factor B_R is given by

$$B_R = \frac{\sum_{J=0,2}^{\infty} g_J(z) \int_{-\infty}^{\infty} \frac{dx}{\sqrt{\pi}} \varphi(x/A)\, e^{-\tau_J \varphi(x)}}{AT_b(\sigma N)} \qquad (8)$$

where

$$\tau_J = \tfrac{1}{2}\, g_J(z_L)\sigma(N_L - N(z))$$

and

$$A = \sqrt{T(z)/T_L} \cdot$$

other quantities that appear in equation (8) are defined in KJ.

Data and theory are within a factor 0.63 agreement below $z \simeq 70$ km altitude. Considering that the overall calibration of the CVF is about ± 50%, and also considering that an overall change of 2.5°K in the temperature profile can cause a 10% change in 4.3 μm zenith radiance, the agreement for $z \leq 70$ km between the data and calculations as shown on Figure 8 is quite good.

The quoted accuracy ± 50% for the CVF calibration allows us to reduce the data by the factor 0.63. In this way data and theory may be brought into agreement in the region $z < 70$ km. Centered at about 82 km there seems to be a contribution of approximately 10^{-9} w cm^{-2} sr^{-1} 4.3 μm zenith radiance data that can not be explained as the result of CO_2 (001) excitation by the standard (KJ) ambient night time thermal mechanisms: collisions, absorption of earthshine and radiative transport. We utilized a steady state source model for $N_2^{\ddagger}$ excitation $QN_2^{\ddagger} \propto x\, e^{-x}$ where $x = e^{-(z-82\ \mathrm{km})/H}$ and where H = 6 km. By adding the radiance predicted by this model to the ambient calculation (either A or B in Figure 8) we achieved an acceptable fit with the data for an integrated $N_2^{\ddagger}$ excitation source $\int dz\, QN_2^{\ddagger} \simeq 0.067$ ergs $N_2^{\ddagger}$ excitation per cm^2 sec. Next we studied the question: What mechanism is responsible for an $N_2^{\ddagger}$ column excitation of about 0.067 ergs/cm^2 sec that occurs in a narrow layer which peaks up at about 82 km altitude?

We considered several mechanisms to account for such a source of $N_2^{\ddagger}$ excitation (see Section 3.2 above). The only mechanism promising enough to warrant discussion here is the $OH^{\ddagger}$ driven mechanism, that is:

$$N_2 + OH(v) \rightarrow N_2^{\ddagger} + OH(v-1) \tag{9}$$

where the $OH^{\ddagger}$ is initially produced via

$$H + O_3 \rightarrow OH^{\ddagger} + O_2 \tag{10}$$

or

$$HO_2 + O \rightarrow OH^{\ddagger} + O_2 \ . \tag{11}$$

There are two reasons for considering this mechanism: (a) The 82 km peak altitude requirement could be nearly satisfied by reaction (9). The altitude dependence for $OH^{\ddagger}$ emission peaks up at $\simeq$ 84 km. We expect then that the altitude where peak quenching of $OH^{\ddagger}$ occurs would be somewhat lower than 84 km. (b) The total energy/cm^2 sec produced by reaction (10) and (11) exceeds the $\simeq$ 0.067 ergs/cm^2 sec which is required to explain the "knee" in the 11 April 1974 data.

We discussed this mechanism with Dr. A. T. Stair. This was very useful since Dr. Stair was able to rapidly identify the most up to date literature on reactions (9) through (11) and on the Einstein coefficients $A_{v''}^{v'}$ for emission by $OH^{\ddagger}$. Thus we were able to do a preliminary calculation of the rate of $N_2^{\ddagger}$ production due to reaction (9).

There are numerous measurements of OH airglow volume emission rates available in the literature (Reference 20, Baker). To investigate the $OH(v) + N_2 \rightarrow N_2^{\ddagger} + OH(v-1)$ hypothesis we arbitrarily selected the airglow OH $\Delta v = 2$ volume emission rate versus altitude $\epsilon(\Delta v = 2, z)$ reported in the literature by Rogers et al. (Reference 21). The measured volume emission rate published in Reference 21 was measured with an instrumental passband that transmits the OH $\Delta V = 2$ sequence bands 4→2, 3→1 and 2→0 (Reference 22). To estimate the corresponding altitude dependent $N_2^{\ddagger}$ production rate $QN_2^{\ddagger}(z) = \epsilon(\Delta v = 2, z) < k_9/A > [N_2]$ requires a knowledge of the rate constants for reactions (9) and (10). For the purpose of our discussion here in Section 3.3 we will label these rate constants k_9 and k_{10}. A knowledge of

the Einstein coefficients $A^{v'}_{v''}$ for radiative decay of OH(v′) to OH(v″) is also required. In the initial analysis we present here we shall neglect production of OH(v) excitations by reaction (11). The rates $k_{10}(v)$ for $2 \leq v \leq 9$ can be obtained from Polanyi et al. (Reference 23). The rates k_9 can be obtained from Streit and Johnston (Reference 24) for $4 \leq v \leq 9$. T. C. James recommended the $A^{v'}_{v''}$ calculated by F. H. Mies (Reference 25).

The value $< k_9/A > [N_2]$ is given by

$$< k_9/A > [N_2] = \sum_{V=1}^{9} \eta_v k_9(v) [N_2] \Big/ \sum_{V=2}^{4} \eta_v A^v_{v-2}$$

where the $\eta_v = [OH(v)]$ are the populations of OH(v). For $v = 9$

$$\eta_v \cong k_{10}(v) \Big/ \left(A^v + k_9(v) [N_2]\right) \qquad (12)$$

where $A^v \equiv \sum_{v''<v} A^v_{v''}$. For successively smaller values of v the η_v are given by

$$\eta_v = \left(k_{10}(v) + k_9(v+1) [N_2] \eta_{v+1} + \sum_{v'>v} \eta_v A^{v'}_v\right) \Big/ (A^v + k_9(v) [N_2]) \quad . (13)$$

For the purpose of completing this preliminary calculation we extrapolated values for $k_{10}(v)$ for $v = 1$ and $k_9(v)$ for $v < 4$ from the data of References 23 and 24, respectively. The data and the extrapolations are shown on Figure 9. We should note that the $k_9(v)$ reported by Reference 24 are $OH^{\ddagger}$ deactivation rates. In their experiment they were not able to trace whether reaction (9) proceeded by vt, vr or vv. In our calculations we assume that the $k_9(v)$ are vv. The results $Q_{N_2^{\ddagger}}(z)$ are shown on Figure 10. The column $N_2^{\ddagger}$ production $\int dz\, Q_{N_2^{\ddagger}} \simeq 0.14$ ergs/cm^2 sec.

In Figure 11 we show a curve labeled "U" which is the component of 4.3 μm zenith radiance that results from the initial $N_2^{\ddagger}$ excitation source shown on Figure 10. The points X shown on Figure 11 are the best fit to the 11 April 1974 4.3 μm zenith radiance data of a linear combination of the ambient radiance curve A and the curve U. The data have been reduced by a

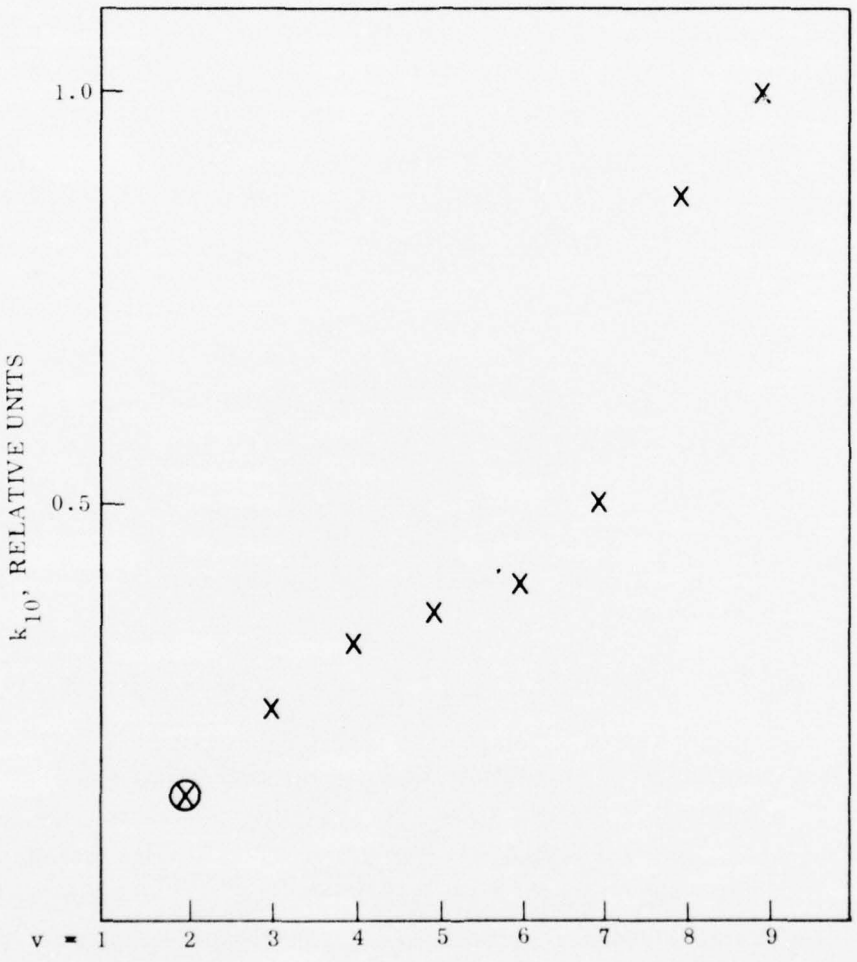

Figure 9a. The X's are data for $k_{10}(v)$ from Reference 23. The ⊗ is the extrapolated value of k_{10} for V = 2.

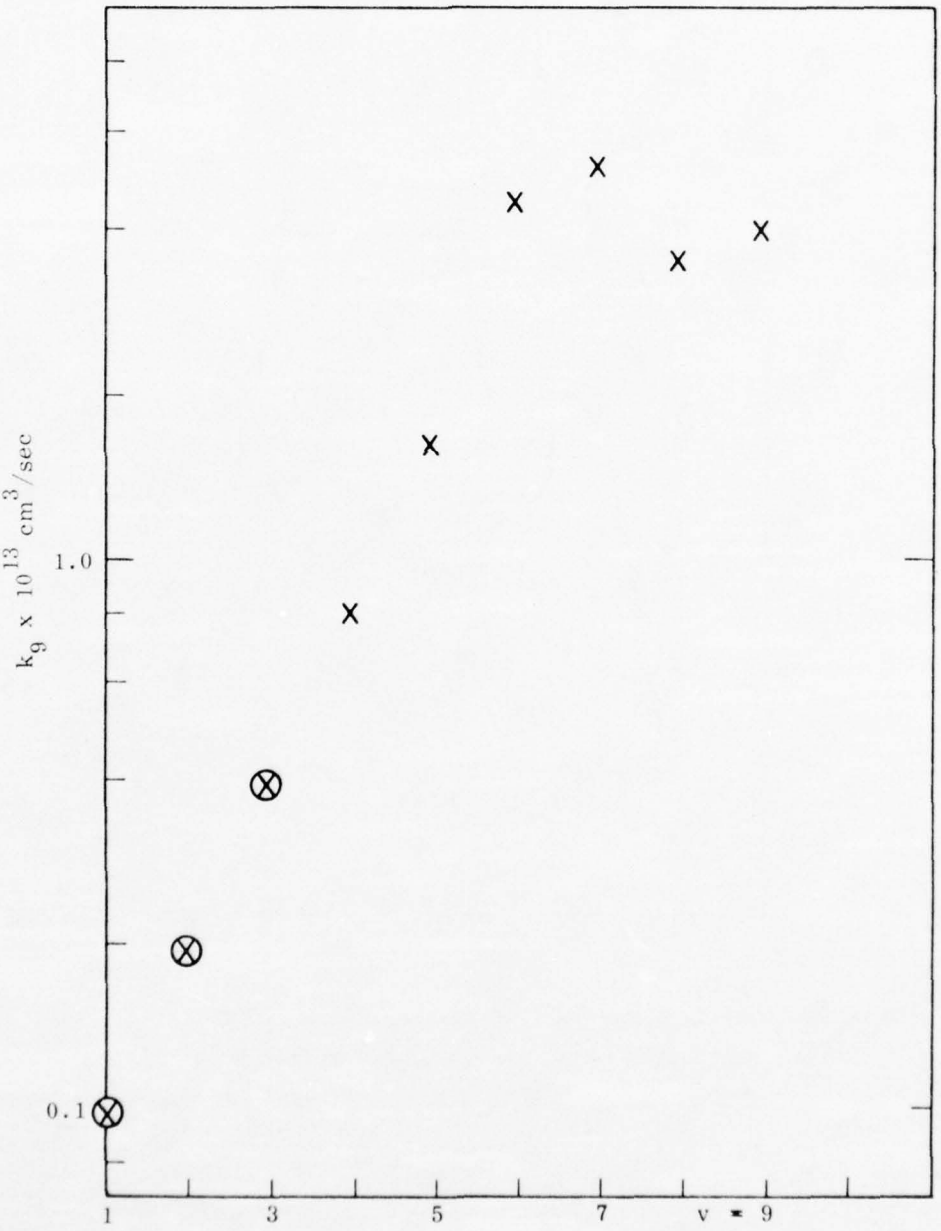

Figure 9b. The X's are data for $k_9(v)$ from Reference 24. The (X)'s are the extrapolated values we used for $k_9(v)$ for $v < 4$.

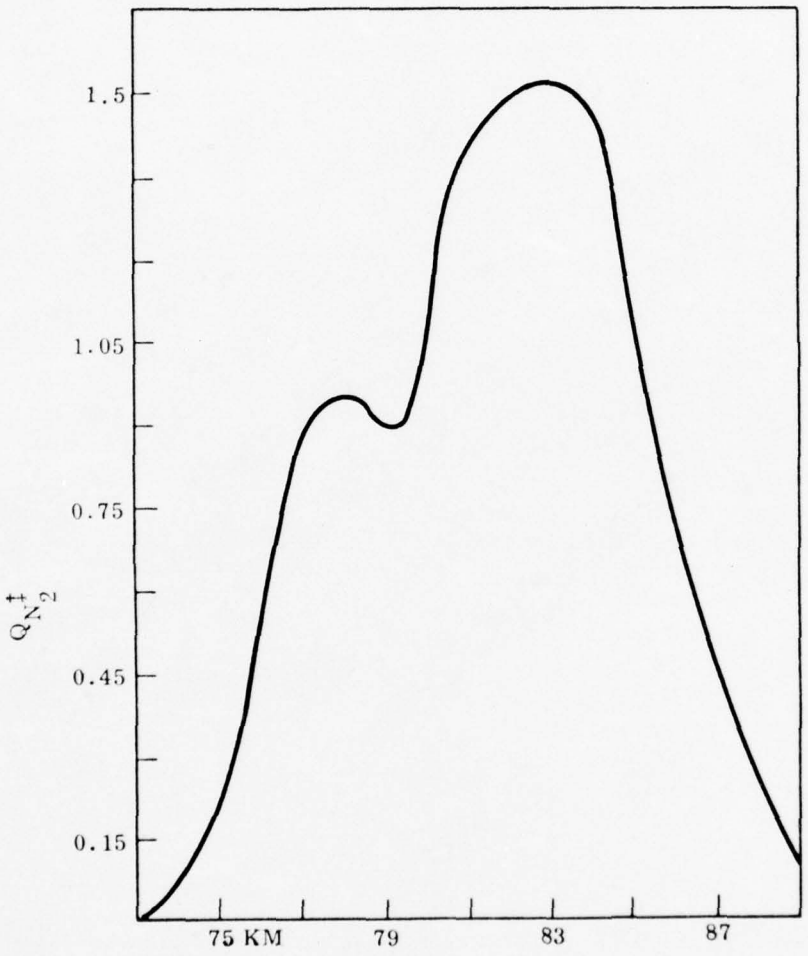

Figure 10. The altitude profile of $Q_{N_2^{\ddagger}}(z)$ the initial excitation of $N_2^{\ddagger}$ via VV transfer from $OH^{\ddagger}$. The units are (14/6) x 10^5 N_2 vibrational quanta/cm^3 sec.

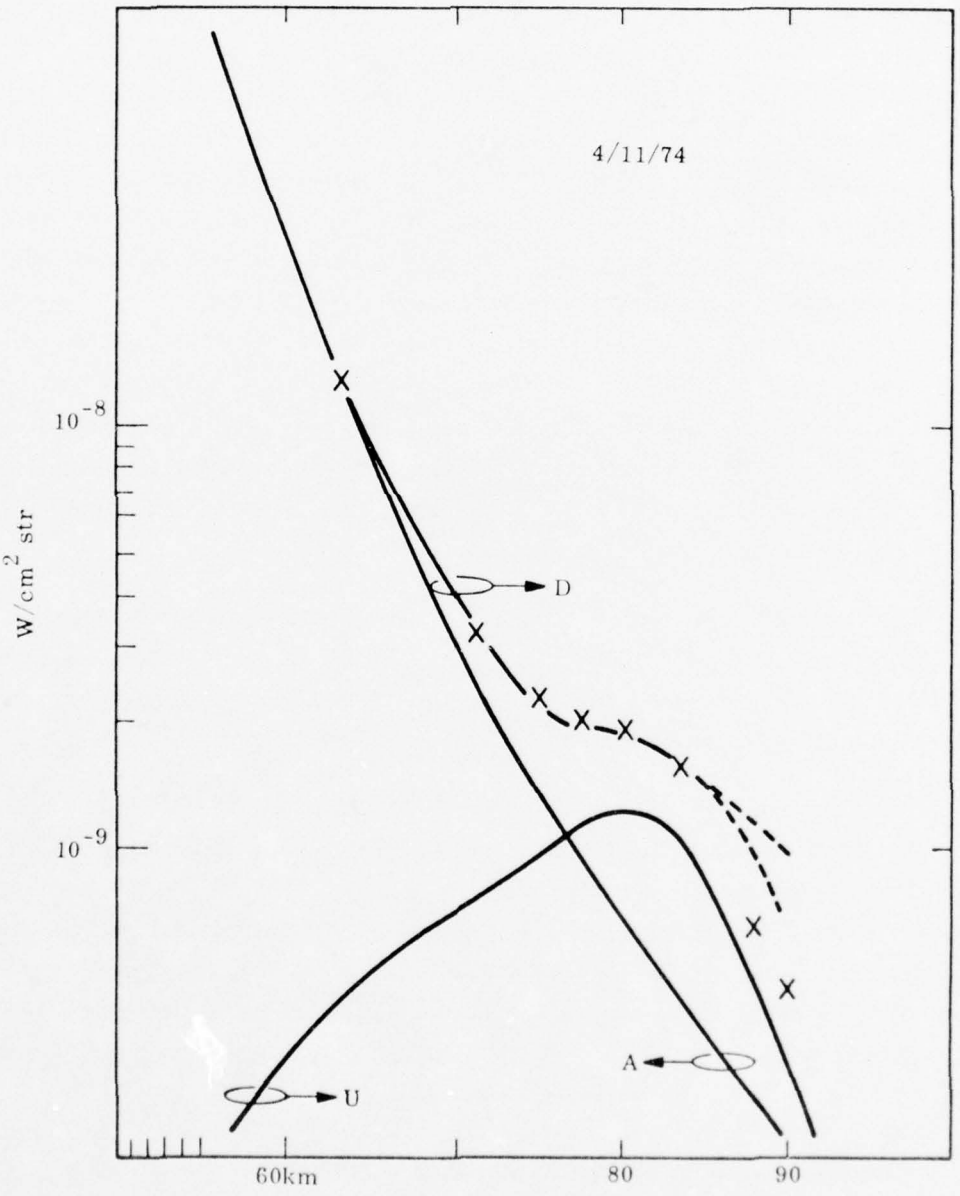

Figure 11. D, The 11 April 1974 data reduced by a factor 0.63
A, Ambient calculation
U, The OH component, it requires OH^+ transfers .078 ergs/cm^2 sec to N_2^+
X, The fit A + U to the data D

factor 0.63 in order to agree with the ambient calculation at the lower end of the altitude scale. The component U had to be multiplied by a factor $\simeq (.078/0.14)$ to achieve the fit shown on Figure 11. This means that, given the altitude dependence for N_2^+ production via vv transfer from $OH^{\ddagger}$ which is shown on Figure 10, that .078 ergs/cm^2 sec $N_2^{\ddagger}$ column production is required to best fit the data. Thus, for the shape of $Q_{N_2^{\ddagger}}(z)$ as the result of reaction (9) as shown on Figure 10 it is required that $\int dz\, Q_{N_2^{\ddagger}} = .078$ ergs/cm^2 sec in order to best fit the data. This is very nearly equal to the 0.067 ergs/cm^2 sec which is required if we arbitrarily set $Q_{N_2^{\ddagger}} \propto xe^{-x}$ as discussed above. The excellent quality of the fit also argues that the altitude dependence of the profile $Q_{N_2^{\ddagger}}(z)$ is what is required to explain the "knee" in the 11 April 1974 data. We believe the excellent quality of the fit partially justifies our assumption that the $k_9(v)$ reported by Streit and Johnston are indeed the result of a vv process rather than vt or vr.

In conclusion, we believe the $OH^{\ddagger} + N_2 \rightarrow N_2^{\ddagger}$ mechanism is most likely responsible for the "knee" in the 11 April 1974 4.3 μm zenith radiance data. The matter should be persued in more detail. This should include a more thorough literature search for more accurate values of $k_9(v)$, $k_{10}(v)$, $A_v^{v'}{}''$ and η_v in the OH airglow.

In the discussion that follows we shall point out corrobative manifestations of what appears to be evidence for an $OH^{\ddagger} + N_2 \rightarrow N_2^{\ddagger} \rightarrow CO_2$ 4.3 μm airglow in data obtained 25 February 1974 and 6 March 1975. The evidence manifested by the 6 March 1975 data is particularly convincing. We have also mentioned that the downleg 27 March 1973 data show similar evidence. We believe that the 27 March 1973 upleg data might also show evidence for the OH related 4.3 μm airglow if these data were to be reexamined.

3.4 Evaluation of Data Obtained 25 February 1974

The 4.3 μm Zenith Radiance Data:

A final version of the 4.3 μm zenith radiance data obtained 25 February 1974 was kindly provided to us by W. Grieder (Reference 26). These data will soon be published.

The Blue Red Input Model (BRIM):

For this event scanning photometer data are most useful for constructing an energy input model. This is because radar (Reference 27) and staring photometer (Reference 28) viewing directions were not exactly coincident with the upleg rocket penetration (entry) at 100 km and certainly not coincident with the downleg 100 km penetration (exit) point. There were available however (Reference 29) tabulations of scanning photometer data taken at the rocket entry and exit points for some 5 minutes prior to launch. These data are shown in Table 2. Inspection of data records obtained prior to 5 minutes prelaunch showed there was not enough energy deposit to significantly impact the observed 4.3 μm radiance profiles.

In order to construct the time histories of energy deposit $q(z,t)$ pertinent for entry and exit points from the photometric data we used methods described by Rees and Luckey (Reference 30). Basically, the ratio $R_{RB} = I_R/I_B$ of the auroral 6300 Å brightness $4\pi I_B$ may be used to obtain the approximate altitude dependence $q(z)$ of the deposition. The absolute magnitude of the 4278 Å brightness may be used to obtain the column deposition $\int dz\, q(z)$.

We will briefly describe the procedure, the quantities $4\pi I_R$ and $4\pi I_B$ are the ground based observables. These are the 6300 Å and 4278 Å auroral ground based observed brightnesses <u>after</u> corrections are made for atmospheric attenuation. From these observables we can form the ratio

$$R_{RB} = I_R/I_B \quad .$$

Next the energy parameter α (units kev) may be obtained via the approximation

$$\ln(\alpha) \cong .3148107 - .6626199 \ln (R_{RB}) \quad .$$

We assume $\underline{\varphi}(E) \propto E\, e^{-E/\alpha}$ so $\bar{E} = 2\alpha$. Approximate values for the altitude $z_p(\bar{E})$ where q is maximum, and for z_L and z_H the altitudes below and above z_p where q is $\frac{1}{2}$ maximum, may be inferred from results presented by Rees (Reference 31). These are

Table 2

The observed (Reference 29) brightness histories $4\pi I_R'(t')$ at 6300 A and $4\pi I_B'(t')$ at 3914 Å for the 25 February 1974 entry and exit points are listed in 2a and 2b below. The time t' is measured backwards from rocket penetration time.

2a

minutes	kR	
t'	$4\pi I_R'$	$4\pi I_B'$
0.	1.2	10.
0.9	1.3	23.
2.03	2.8	53.
2.28	2.1	53.
3.15	1.6	32.
3.62	2.2	45.
4.28	1.5	16.
4.97	1.2	16.
5.20	1.4	6.
6.10	0.8	3.

2b

minutes	kR	
t'	$4\pi I_R'$	$4\pi I_B'$
0.	1.1	6.
0.88	1.3	20.
1.33	2.1	115.
1.83	1.0	10.
2.67	0.8	6.
3.57	1.2	11.
4.03	2.7	57.
6.17	2.2	11.
6.85	1.6	6.
11.00	0.6	2.

$\bar{E}$ (kev)	(km) z_L	z_p	z_H
1.00	156	170	235
1.65	135	146	185
5.00	110	117	125
40.00	88	92	100

For given $\bar{E} = 2\alpha$ we can interpolate to get z_L, z_p and z_H. We define $H_L = (z_p - z_L)/\sqrt{\ln(2)}$ and $H_H = (z_H - z_p)/\ln(2)$. We approximate $q(z)$ by

$$q(z) \cong q_o \, e^{-(z-z_p)/H_H} \quad \text{for } z > z_p$$

$$q(z) \cong q_o \, e^{-[(z_p-z)/H_L]^2} \quad \text{for } z < z_p \, ,$$

and

$$q_o = \frac{g_H \, g_L}{g_H + g_L} \int dz \; q(z) \, ,$$

where g_L and g_H are defined by

$$1 \equiv g_L \int_o^{z_p} e^{-[(z_p-z)/H_L]^2} \, dz \, ,$$

and

$$1 \equiv g_H \int_{z_p}^{\infty} e^{-(z-z_p)/H_H} \, dz \, .$$

We get $\int dz \; q$ from $4\pi \, I_B$ via $\int dz \; q = 4\pi \, I_B/\epsilon_b$ and an approximate analytic expression for ϵ_b (units kR of 4278 Å/erg deposition) may be inferred from Reference 30, this

$$\epsilon_b = .208 + .003 \ln(\alpha/10.)/\ln(5.212) \quad \text{for } \alpha > 10 \text{ kev}$$

and

$$\epsilon_b = .16 + .048 \ln(\alpha)/\ln(10) \quad \text{for } \alpha < 10 \text{ kev} \, .$$

Thus for any pair of values $4\pi\ I_R$ and $4\pi\ I_B$ an approximation to q(z) may be obtained. We note that the scanning photometer values $4\pi\ I'_R$ and $4\pi\ I'_B$ listed for the entry and exit points in Reference 29 are uncorrected for atmospheric attenuation, and the I'_B listed in Reference 29 are for 3914 Å not 4278 Å radiation. Thus to get the attenuation corrected values for $4\pi\ I_R$ and $4\pi\ I_B$ for 6300 Å and 4278 Å we apply a multiplicative correction to the observations $4\pi\ I'_R$ and $4\pi\ I'_B$

$$I_R = f_R\ I'_R$$
$$I_B = f_B\ I'_B/3.7 \ .$$

We used the values $f_R = 1.26$, $f_B = 2.09$ for the entry point and $f_R = 1.38$, $f_B = 2.83$ for the exit point. These values were calculated on the basis of atmospheric Rayleigh and averaged aerosol attenuation data that are listed by Elterman (Reference 32).

In Figure 12 we show two deposition profiles q(z) for 25 February 1974, 7:38 UT. at the entry point. One of these is calculated via $q(z) \cong \alpha_c\ n_e^2$ where the electron density n_e is obtained from the incoherent scatter radar data as reported in Reference 27 and therefore is actually the value of n_e that obtains at a position displaced by about 15 km from the rocket entry point. We use a value for effective recombination coefficient α_c obtained from Wickwar et al. (Reference 33). The other profile is obtained from the values $4\pi\ I'_R \cong 1.9$ kR and $4\pi\ I'_B \cong 40$ kR as reported for the entry point for 25 February 1974, 7:38 UT in Reference 29. The agreement in q(z) determined from these independent data is satisfactory considering that there is some lateral separation associated with the applicability of the two data sets, and considering there is uncertainty in the factors f_R and f_B which are strongly dependent on conditions of atmospheric visibility. To our knowledge atmospheric visibility was not monitored, hence in lieu of anything better, we were forced to use the averaged model atmospheric aerosol attenuation that is listed in Reference 32.

In order to obtain the 25 February 1974 4.3 μm auroral zenith radiance profiles it is necessary to generate the auroral inhomogeneous terms for equations (6) above, these are

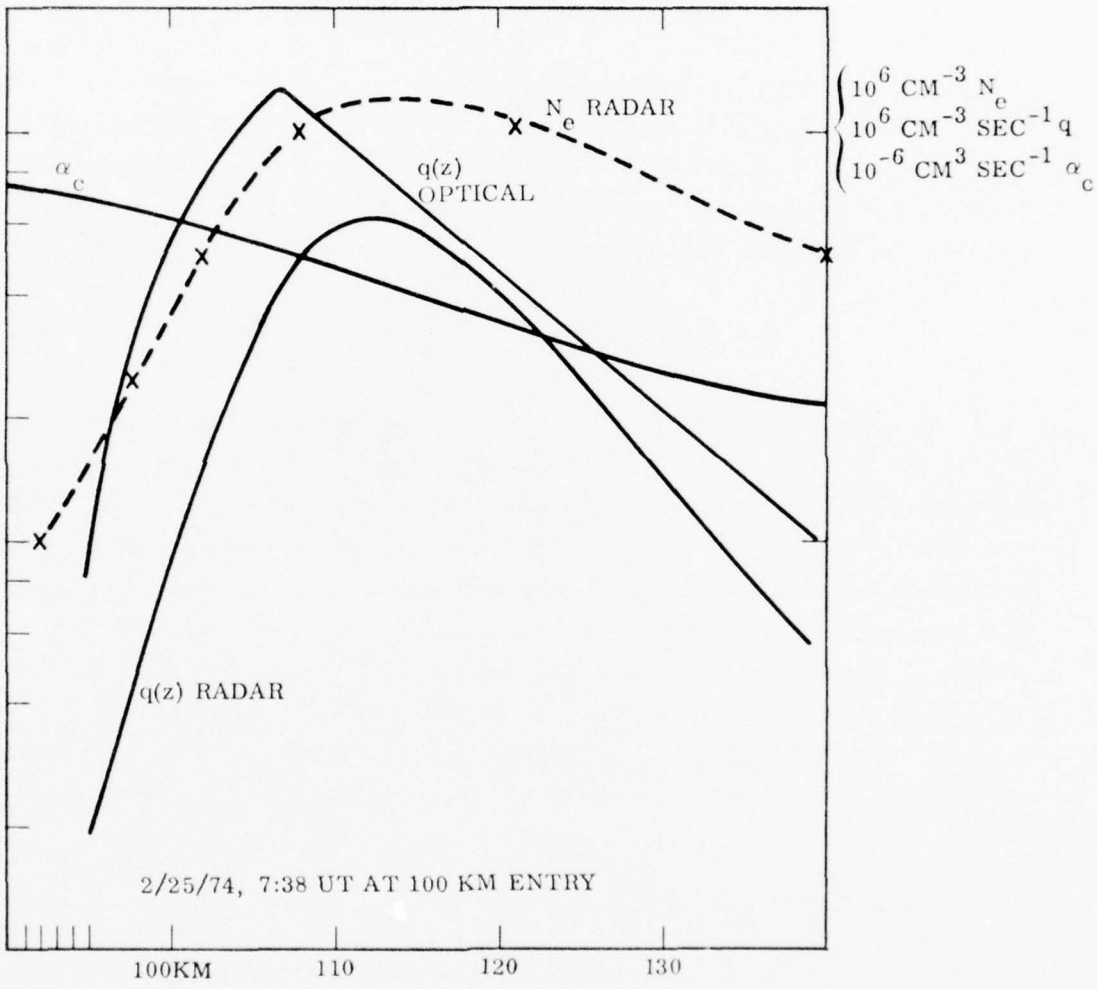

Figure 12. q(z) for 7:38 UT, 25 February 1974 at the 100 km entry point as derived from (1) the optical data in Reference 29 and (2) radar data N_e from Reference 27 and the effective recombination coefficient α_c from Wickwar et al. (Reference 33).

$$\eta_N(z_i,t') = \epsilon q(z_i,t')/[N_{2i}] \quad .$$

Thus it is necessary to generate a time history $q(z_i,t')$ of energy deposit in the vicinity of the entry and exit points at each of 26 altitude mesh points z_i. The time history should extend back in time for about 1 hour or at least until auroral activity has become negligible. In order to obtain the TDT solution for equations (6) it is necessary to compute the integrals

$$\eta_{ij} = \left(\frac{\epsilon}{[N_2]_i}\right)\int_o^\infty dt' \, e^{-\lambda_j t'} \, q(z_i,t') \quad . \tag{14}$$

In numerically computing the integrals in equation (14) it is necessary to evaluate $q(z_i,t_k')$ for each integration mesh point t_k'. This was achieved by determining $4\pi \, I_R'(t_k')$ and $4\pi \, I_B'(t_k')$ by linear interpolation from the approximate data sets which are listed in Tables 2a and 2b. These approximate data sets are based on the photometric data appropriate for entry and exit points that are reported in Reference 29. Next $q(z_i,t_k')$ may be evaluated from $4\pi \, I_k'(t'_k)$ and $4\pi \, I_B'(t_k')$ as described above. If t_k' is greater than the largest value t'_{max} that is listed in Table 2a or 2b, then $4\pi \, I_R(t'_{max})$ and $4\pi \, I_B(t'_{max})$ are used to generate $q(z_i,t_k')$. By inspection of the data sets in Tables 2a and 2b one sees that this procedure for $t_k' > t'_{max}$ accounts for preauroral drizzle.

The solution of equations (6) then is

$$f_i = \sum_{j=1}^{52} K_{ij} \sum_{k=27}^{52} (K_{jk}^{-1} \eta_{kj}) \quad .$$

For a given altitude mesh point z_i the fractional populations $f_i(z_i) = [001]_i/[CO_2]_i$ anf $f_N(z_i) = [N_2^\ddagger]_i/[N_2]_i$ are given by

$$f_1(z_i) = f_i$$

and

$$f_N(z_i) = f_{i+26} \quad .$$

The fractional populations of the weak bands are determined from equations (6) with $\eta_j(z_i)$ set to zero. Then the zenith radiance in each band R_j may be computed via equation (8b) above.

In Table 3 we show the results for the 25 February 1974 upleg auroral radiance components R_j in each band, and for ΣR_j the sum of these radiances, which are obtained by this procedure. These results were generated for a value $\epsilon = 15.4$ (N_2 vibrations/ionization) although we shall see below that it is necessary to use $\epsilon \cong 15.2$ to achieve a best fit to the 25 February 1974 data.

In our discussions in this report whenever we refer to the radiance component due to a given mechanism (auroral, airglow, ambient thermal) we always are referring to ΣR_j the sum over all the CO_2 ν_3 4.3 μm bands.

We draw your attention back to Table 3 in order to make one last point. The bands j = 10 and 11 originate from the upper levels $02^0 1$ and $10^0 1$, these levels may decay to 000 and emit 2.7 μm radiation in the process. The relative emission at 2.7 μm and 4.3 μm is expected theoretically (Reference 8) to be 4% and 96% respectively. By inspection of Table 3 one sees we predict the 4.3 μm radiance in these j = 10 and 11 bands is $\simeq 10^4$ less than in the fundamental CO_2 (001) → CO_2 (000) j = 1 band in the region z > 90 km. Hence 2.7 μm zenith radiance from these bands in the z > 90 km region will be at least 10^5 less than the 4.3 μm zenith radiance in this altitude region. We conclude that the slowly decaying component of 2.7 μm radiance which has been noted (Reference 35) in auroral data probably does <u>not</u> come from the N_2, CO_2 vibration transfer mechanism

$$N_2^{\ddagger} + \begin{Bmatrix} CO_2\ (100) \\ CO_2\ (02^0 0) \end{Bmatrix} \rightarrow N_2 + \begin{Bmatrix} CO_2\ (10^0 1) \\ CO_2\ (02^0 1) \end{Bmatrix} \qquad (15)$$

followed by radiative emission at 2.7 μm

$$\begin{Bmatrix} CO_2\ (10^0 1) \\ CO_2\ (02^0 1) \end{Bmatrix} \rightarrow CO_2\ (000) + h\nu_{2.7\ \mu m}$$

<u>unless</u> there is an unexpected quirk in the relative magnitudes of the vv reaction rate constants for vibration transfer between N_2 and the CO_2 ground

Table 3a. The sum of the 4.3 μm auroral component of zenith radiance in all of the CO_2 ν_3 bands $\sum_{j=1}^{11} R_j$, the 4.3 μm auroral radiance component in the fundamental band R_1, and the 4.3 radiances in the fluorescent bands j = 10 and 11 are tabulated here. These auroral radiances are calculated for q(z,t) given by our BRIM model for the 25 February 1974 upleg. A value ϵ=15.4 (N_2^+/ionization) was used in compiling these although we show below that ϵ = 15.24 is required to best fit the data.

	w cm^{-2} sr^{-1}			
z (km)	ΣR_j	R_1	R_{10}	R_{11}
.1400+03	.7178-10	.7151-10	.2907-15	.2078-15
.1072+03	.3993-08	.3938-08	.5908-13	.3460-13
.9884+02	.1043-07	.1015-07	.3157-12	.1595-12
.9508+02	.1040-07	.1009-07	.3579-12	.1779-12
.9252+02	.9485-08	.9167-08	.3779-12	.1906-12
.9098+02	.8884-08	.8528-08	.4308-12	.2152-12
.9018+02	.8557-08	.8192-08	.4414-12	.2184-12
.8818+02	.7673-08	.7258-08	.5091-12	.2468-12
.8384+02	.5375-08	.4758-08	.8797-12	.4130-12
.8022+02	.3549-08	.2969-08	.1077-11	.4907-12
.7768+02	.2595-08	.2087-08	.1347-11	.6183-12
.7605+02	.2177-08	.1524-08	.1678-11	.7765-12
.7520+02	.1977-08	.1398-08	.1852-11	.8614-12
.7385+02	.1709-08	.1032-08	.2127-11	.9979-12
.7060+02	.1192-08	.5458-09	.2945-11	.1411-11
.6659+02	.7944-09	.2923-09	.3641-11	.1794-11
.6345+02	.5628-09	.1823-09	.3967-11	.2021-11
.6137+02	.4291-09	.1345-09	.3740-11	.1960-11
.6026+02	.3857-09	.1153-09	.3839-11	.2055-11
.5935+02	.3507-09	.1015-09	.3836-11	.2093-11
.5719+02	.2710-09	.7292-10	.3505-11	.2007-11
.5467+02	.1949-09	.5026-10	.2896-11	.1772-11
.5254+02	.1533-09	.3601-10	.2633-11	.1731-11
.5103+02	.1218-09	.2856-10	.2196-11	.1522-11
.5020+02	.1091-09	.2496-10	.2055-11	.1469-11
.5000+02	.1062-09	.2410-10	.2023-11	.1458-11

Table 3b. The 4.3 μm auroral radiance components R_j in the bands j = 2 through 9, computed via the same q(z,t) as described in the caption for Table 3a, are listed here.

	k_2 w cm^{-2} sr^{-1}							
(km)	2	3	4	5	6	7	8	9
.1400+03	.1397-12	.4955-13	.8584-14	.6295-13	.2417-15	.7571-16	.1337-16	.5534-15
.1072+03	.2985-10	.1052-10	.1819-11	.1224-10	.4696-13	.1472-13	.2601-14	.1016-12
.9884+02	.1516-09	.5345-10	.9244-11	.6318-10	.2425-12	.7602-13	.1343-13	.5056-12
.9508+02	.1664-09	.5875-10	.1017-10	.7119-10	.2736-12	.8582-13	.1517-13	.5684-12
.9252+02	.1710-09	.6047-10	.1047-10	.7522-10	.2897-12	.9089-13	.1607-13	.6037-12
.9048+02	.1963-09	.6744-10	.1169-10	.8543-10	.3295-12	.1034-12	.1830-13	.6848-12
.9018+02	.1947-09	.6903-10	.1197-10	.8744-10	.3373-12	.1059-12	.1874-13	.6986-12
.8818+02	.2207-09	.7839-10	.1361-10	.1007-09	.3882-12	.1221-12	.2163-13	.7982-12
.8384+02	.3114-09	.1114-09	.1943-10	.1715-09	.6641-12	.2100-12	.3736-13	.1352-11
.8122+02	.2583-09	.9076-10	.1574-10	.2114-09	.8027-12	.2573-12	.4626-13	.1615-11
.7768+02	.2325-09	.8033-10	.1383-10	.2568-09	.9943-12	.3227-12	.5861-13	.2010-11
.7605+02	.2478-09	.8733-10	.1519-10	.2959-09	.1227-11	.4007-12	.7313-13	.2504-11
.7520+02	.2483-09	.8860-10	.1551-10	.3084-09	.1343-11	.4401-12	.8053-13	.2764-11
.7385+02	.2453-09	.8972-10	.1591-10	.3170-09	.1526-11	.5027-12	.9242-13	.3177-11
.7050+02	.2382-09	.9738-10	.1834-10	.2804-09	.2030-11	.6757-12	.1252-12	.4421-11
.6659+02	.1973-09	.9548-10	.1987-10	.1751-09	.2422-11	.8142-12	.1519-12	.5520-11
.6345+02	.1534-09	.8721-10	.2027-10	.1039-09	.2620-11	.8887-12	.1667-12	.6105-11
.6137+02	.1186-09	.7560-10	.1939-10	.6639-10	.2555-11	.8737-12	.1647-12	.5833-11
.6026+02	.1068-09	.7243-10	.1963-10	.5579-10	.2662-11	.9145-12	.1728-12	.6050-11
.5935+02	.9688-10	.6876-10	.1963-10	.4802-10	.2720-11	.9387-12	.1777-12	.6104-11
.5719+02	.7335-10	.5764-10	.1907-10	.3289-10	.2740-11	.9572-12	.1821-12	.5720-11
.5467+02	.5014-10	.4264-10	.1712-10	.2147-10	.2636-11	.9399-12	.1806-12	.4886-11
.5254+02	.3861-10	.3348-10	.1591-10	.1691-10	.2753-11	.1005-11	.1952-12	.4601-11
.5103+02	.2891-10	.2584-10	.1384-10	.1327-10	.2609-11	.9728-12	.1911-12	.3935-11
.5020+02	.2531-10	.2279-10	.1301-10	.1196-10	.2602-11	.9834-12	.1945-12	.3732-11
.5000+02	.2455-10	.2214-10	.1263-10	.1166-10	.2601-11	.9864-12	.1955-12	.3688-11

state species (000), (100) and (020). This quirk may be explained as follows, in our calculations (equations (1) and (6)) we have assumed the rate constant for

$$N_2^{\ddagger} + [j] \rightleftharpoons N_2 + [\nu_3 j]$$

to be identical with the vv exchange rate k_2 for

$$N_2^{\ddagger} + CO_2\ (000) \rightleftharpoons N_2 + CO_2\ (001) \quad .$$

The rate k_2 is about 10^{-3} kinetic, thus if the largest conceivable (if not reasonable) rate is used for reaction (15), i.e. $10^3\ k_2$, then 2.7 μm as the result of the N_2, CO_2 vibration exchange mechanism will be approximately 10^2 less than the 4.3 μm radiance. This is close enough to the apparent long term 2.7 μm auroral component data requirement (Reference 35) that the long term 2.7 μm auroral radiance is a factor 10 less than the 4.3 μm radiance so that perhaps the N_2, CO_2 vibration exchange mechanism for producing auroral 2.7 μm radiance might warrant a little more careful attention.

25 February 1974 Upleg Data Evaluation:

In Figure 13 we show the 25 February 1974 upleg 4.3 μm zenith radiance data compared with our calculations. The data are the curve labelled D. The auroral component of 4.3 μm zenith radiance A_u is calculated from a TDT solution obtained from the time history of photometric data in Table 2a via the BRIM capability to generate $q(z,t')$ as discussed above. With this BRIM generated model $q(z,t')$ it is necessary to use $\epsilon = 15.24$ (N_2 vibrational quanta/ionization) to obtain the magnitude of Au as shown.

Our calculation for the 4.3 μm zenith radiance component due to ambient thermal mechanisms, collisions and absorption of earthshine, must be multiplied by the factor 10 to keep it on scale in Figure 13. This component is labelled A_m(x10). The ambient thermal radiance A_m is calculated on the basis of ASL meteorological rocket data on atmospheric temperature and density obtained 25 February 1974 which were kindly provided by R. O. Olsen (Reference 34). These data extended up to 60 km altitude. The complete temperature profile was obtained by smoothly extrapolating from the ASL data near 60 km to the Groves 65° N March mesopause temperature model exactly as was done to obtain

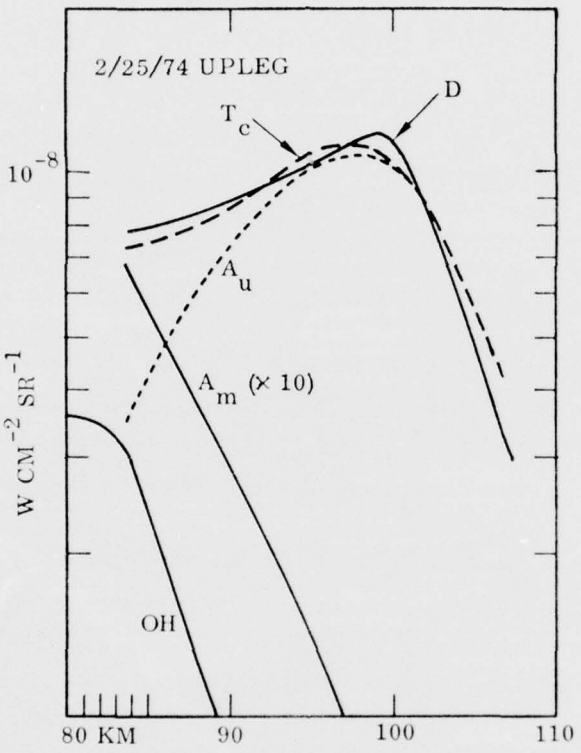

Figure 13. 25 February 1974 upleg 4.3 μm zenith radiance data (Curve D) are compared with curves A_u the BRIM input calculation for the auroral component of zenith radiance, OH the calculated component due to vibration transfer from $OH^{\ddagger}$, A_m(x10) the ambient thermal component multiplied by a factor 10 so that it is on scale, and T_c the sum OH + A_u + A_m.

a temperature profile for the 11 April 1974 data as illustrated by Figure 7 above.

We note the sum $A_u + A_m$ is 4.3×10^{-9} w cm^{-2} sr^{-1} at z = 84 km but the datum at z = 84 km is 7.8×10^{-9} w cm^{-2} sr^{-1}. If we compute an $OH^{\ddagger} \xrightarrow{VV} N_2^{\ddagger}$ CO_2 4.3 μm radiance component from an $N_2^{\ddagger}$ excitation source that is obtained by multiplying the $QN_2^{\ddagger}(z)$ shown on Figure 10 by a factor .93 we obtain the 4.3 μm zenith radiance component which is labelled OH on Figure 13. This requires $E_{TV} \equiv$ 0.13 ergs/cm^2 sec of vibrational energy transfer from $OH^{\ddagger}$ to N_2.

The curve labelled T_c (for theoretical composite) is the sum of the curves A_u + OH + A_m. The fit with the data is reasonable as are the physical requirements ε = 15.24 N_2 vibration quanta produced per ionizations event and that $OH^{\ddagger}$ transfers 0.13 ergs/cm^2 sec of vibration energy to N_2.

We looked at several alternate energy deposit models for the 25 February 1974 upleg. The total integrated energy input was held constant, that is at any time t′ it was required that $\int dz\, q(z,t') = 4\pi I_B(t')/\varepsilon_b(t')$. The two alternate models differed from the model we described above only in the z dependence of q(z,t).

In one case we used a quartic fit for the bottom of q(z,t′) rather than the parabolic bottom as described above. That is, for $z < z_p$ we used

$$q = q_o\, e^{-[(z_p - z)/H_L]^4}$$

where

$$H_L = (z_p - z_H)/\sqrt[4]{\ln(2)} \quad .$$

We also used an input model g(t′) q(z) where q(z) is the radar derived $q_R(z)$ shown in Figure 12 and with g(t′) such that

$$g(t') \int dz\, q_R(z) = 4\pi I_B(t')/\varepsilon_b(t') \quad .$$

Results for the values of physical parameters required to achieve a best fit to the data by adding $A_u + A_m$ + OH are listed below:

Input Model		$\epsilon\left(\frac{N_2^+}{\text{ionization}}\right)$	$E_{TV}\left(\frac{\text{ergs}}{\text{cm}^2\ \text{sec}}\right)$
BRIM	Parabolic Bottom	15.24	.131
	Quartic Bottom	21.60	.139
	Radar q(z)	19.80	.093

These results are reasonably consistent. However, the modeling of the 4.3 μm auroral zenith radiances for rather narrow discrete arcs such as is the case for the 25 February 1974 upleg would certainly be more accurate if lateral transport effects such as lateral radiative photon diffusion and the transport of N_2^+ by winds were accounted for. To account for wind transport of N_2^+ requires that some information on wind fields needs to be provided. It should be possible to obtain some ideas on wind velocities in the region of the OH airglow layer peak (84 km) and the Na airglow layer peak (92 km) from Sears' 3 beam photometric data. It would be a useful exercise to obtain these wind data to see what is the impact on the modeling of the 4.3 μm zenith radiance data.

25 February 1974 Downleg Data Evaluation:

In Figure 14 we show the 25 February 1974 downleg 4.3 μm zenith radiance data compared with our calculations. The data are the curve labelled D. The curve D is perforated for $z < 85$ km. The rocket tipped over at 85 km and we are cautious with regard to analysis of the data for $z < 85$ km. For this reason we did not attempt to fit the data for $z < 85$ km, but instead concentrated on analysis of the data in the region $z > 85$ km.

The curve labelled BRIMIN is the auroral zenith radiance component calculated via a TDT solution for an input model $q(z,t')$ which is generated by our BRIM capability from the photometric data listed in Table 2b. A value $\epsilon = 16.2$ (N_2^+/ionization) was required to achieve the fit shown on Figure 14. This is quite consistent with the results achieved on analysis of 25 February 1974 upleg data as reported above.

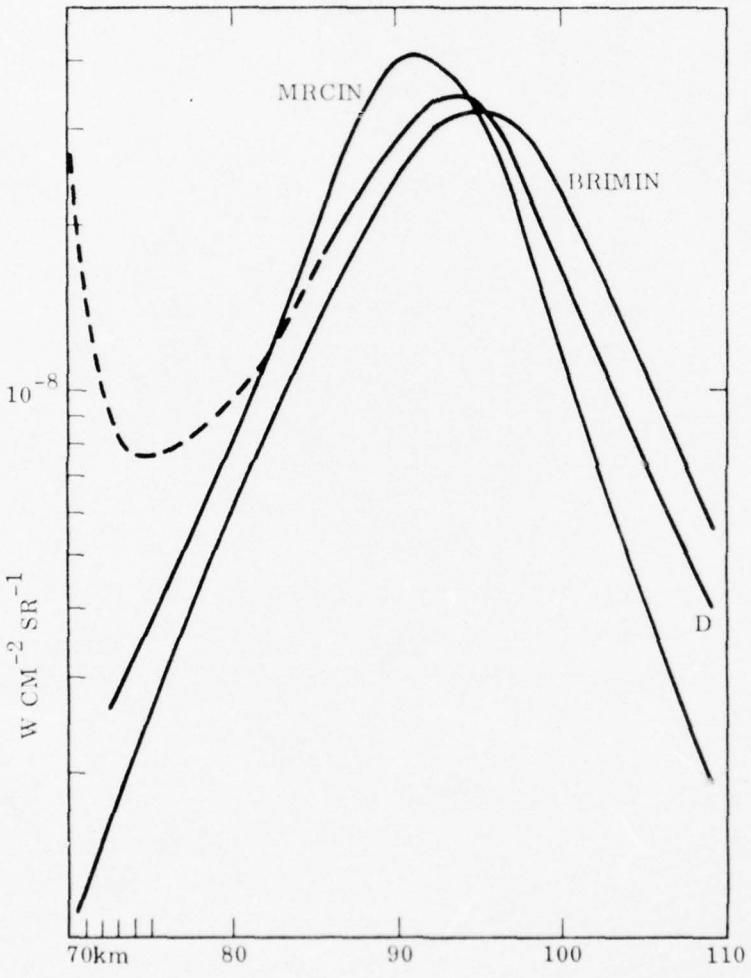

Figure 14. A comparison of the 25 February 1974 downleg data (Curve D) and calculations (Curve BRIMIN) based on our BRIM energy input model, and calculations (Curve MRCIN) based on the MRC input model. Values ϵ = 16.2 and 9.6 (N_2/ionization) are required for the two input models respectively.

We also calculated an auroral component which is the curve labelled MRCIN on the basis of the 25 February 1974 downleg input model proposed by Tarr and Archer (Reference 12). The published MRC 25 February 1974 downleg input model is for the differential spectrum $\underline{\varphi}$ (E) of the precipitating electrons which predose the air at the 25 February 1974 downleg 100 km penetration point. The electrons are assumed to be isotropic in pitch angle. As a function of t′ (in sec) the MRC input model is

$$\underline{\varphi}_D = 5.2 \times 10^{-7}\, e^{-E/4} \text{ for } \begin{cases} 0 < t' < 70 \\ t' > 95 \end{cases}$$

and

$$\left.\begin{aligned} \underline{\varphi}_A &= 10^{-8} \text{ for } E < 35 \text{ kev} \\ \underline{\varphi}_A &= 0 \quad \text{for } E > 35 \text{ kev} \end{aligned}\right\} \text{ for } 70 < t' < 95$$

The units of $\underline{\varphi}$ are (electrons kev^{-1} sec^{-1} cm^{-2} ster^{-1}) and E is in kev. W. Francis kindly agreed to exercise the LMSC AURORA code to generate deposition profiles $q_D(z)$ and $q_A(z)$ from the $\varphi_D(E)$ and $\varphi_A(E)$. Thus

$$q(z,t') = q_D(z) \quad \begin{cases} 0 < t' < 70 \\ t' > 95 \end{cases}$$

and

$$q(z,t') = q_A(z) \qquad 70 < t' < 95$$

served as our version of the MRC input model $q(z,t')$. A value $\varepsilon = 9.6$ (N_2^+/ionization) was required to achieve the fit shown on Figure 14. This is quite reasonable considering the difficulties that are involved in determining for what amount of time the intense hard $\underline{\varphi}_A$ spectrum really does dose the air in 25 February 1974 downleg region.

The BRIM input model calculation peaks up at altitudes higher than does the data, the MRC input model calculation at altitudes lower than does the data. Values of ε are reasonable in either case. It would appear the actual input $q(z,t')$ lies somewhere between the 2 models.

Conclusions:

We were able to consistently model the upleg and downleg data via energy input models generated from photometric data by our BRIM capability. A value ϵ = 15 to 20 ($N_2^{\ddagger}$/ionization) was necessary. The BRIM model appears to generate $q(z,t')$ that are too hard on the upleg and too soft on the downleg. This suggests we used too small a value for atmospheric aerosol attenuation in applying attenuation corrections to the photometric data obtained from Reference 29. Applying a larger aerosol correction would mildly reduce the values for ϵ that would be required to achieve a good fit to the data. The analysis on the 25 February 1974 data has advanced to the state that any further modeling work that might be done on the 25 February 1974 data will have to include lateral transport by winds and by lateral radiative diffusion, in order to be useful.

The upleg 25 February 1974 data in the region $z < 90$ km suggest that there is present in the data a component of 4.3 μm zenith radiance that would be caused by a vibration transfer E_{IV} of about 0.13 (ergs/cm^2 sec) from $OH^{\ddagger}$ to N_2. Confirmation from the downleg data is not readily feasible (1) the auroral component of the downleg data is about 3.3 times brighter than on the upleg, a fact which in itself would tend to wash out $OH^{\ddagger}$ driven effects for $z < 90$ km and (2) the data may yet be suspect for $z < 85$ km. We believe some further analysis of the effect of the rocket aspect angle on the observed radiance may be warranted.

Finally, the MRC downleg input model seems reasonable, although the $\varphi_A(E)$ of this model appears to be somewhat too hard.

3.5 Analysis for Data Obtained 6 March 1975

Twilight and night time 4.3 μm zenith radiance data were obtained in two rocket borne radiometer experiments launched 03:43:00.028 and 06:16:30.020 UT 12 March 1975 from the Poker Flat, Alaska, rocket range. In the twilight shot the shadow height (uncorrected for atmospheric refraction) was about 12 km, so for this shot the 4.3 μm zenith radiance data were obtained in a

sunlit atmosphere for which the solar zenith angle was greater than 90°. Data related to this solar zenith angle and shadow height (refraction corrected) which were kindly provided by Gene Ware and D. Baker (Reference 37) are shown in Table 4. Magnetic and auroral conditions were quiet at the times the rockets were in orbit.

The 4.3 μm zenith radiance obtained on these rocket shots have been published by Ulwick and Stair in Reference 14. We show these data on Figure 15. The data set marked D_t is twilight data and the data set marked D_N is the night time data.

Theoretical curves for various mechanisms are also plotted on Figure 15. We shall discuss these in turn and arrive at what we believe to be a consistent picture for the interpretation of the data.

The curve labelled A_m is our calculation for the radiance component due to ambient thermal mechanisms, collisions, and absorption of earthshine. A_m is calculated on the basis of an atmospheric temperature profile derived from ASL meteorological rocket data which were obtained on 6 March 1975 up to about 60 km altitude (Reference 34) and then by interpolation from 60 km up to altitude 85 km where the OH rotational temperature 208° K, appropriate for 06:18 UT 6 March 1975 were obtained from Ware et al. (Reference 38). The curve A_m does not fit the data set D_N.

On the basis of our experience in dealing with the 11 April 1974 data, the 27 March 1973 downleg (and perhaps upleg) data and the 25 February 1974 upleg data, we were tempted to fit to the night time data D_N a radiance component due to vibration transfer from $OH^{\ddagger}$ to N_2. The result is the dashed curve labelled OH_N. With the radiometer calibration as stated in Reference 14 this fit requires E_{TV} = 0.354 ergs cm^{-2} sec^{-1} of transfer of vibrational energy to N_2 from $OH^{\ddagger}$.

Now let us consider the sunlit data D_t. Our prediction for the zenith radiance component which results from 2 sunlight-driven mechanisms, namely

Table 4. An exerpt of data provided by Reference 37.

6 MAR 1975

LOOK ANGLES TO THE SUN FROM POKER FLAT, ALASKA

COORDINATES FOR POKER FLAT, ALASKA
LATITUDE = 65.12925 DEGREES NORTH
LONGITUDE = 147.48292 DEGREES WEST
ELEVATION = 0.20413 KILOMETERS

COORDINATES FOR THE SUN AT 00H 6 MAR 1975 UT
GREENWICH SIDERIAL TIME = 10H 52M 25.720S
RIGHT ASCENSION = 23H 3M 57.790S 222.770S DELTA
DECLINATION = -5DEG -59M -31.600S 1394.300S DELTA

UT HR:MIN:SEC	AZIMUTH DEGREES	ELEVATION DEGREES	ZENITH ANGLE DEGREES	SHADOW HEIGHT KM
3:20:00	258.12	-1.04	91.04	0.00
3:30:00	260.38	-2.07	92.07	0.86
3:40:00	262.64	-3.12	93.12	3.82
3:50:00	264.90	-4.17	94.17	8.92
4:00:00	267.16	-5.22	95.22	16.21
4:10:00	269.43	-6.27	96.27	25.68
4:20:00	271.70	-7.33	97.33	37.36
4:30:00	273.97	-8.38	98.38	51.24
4:40:00	276.25	-9.43	99.43	67.32
4:50:00	278.54	-10.48	100.48	85.56
5:00:00	280.84	-11.52	101.52	105.94
5:10:00	283.16	-12.55	102.55	128.40
5:20:00	285.49	-13.57	103.57	152.90
5:30:00	287.83	-14.58	104.58	179.36
5:40:00	290.19	-15.58	105.58	207.70
5:50:00	292.57	-16.56	106.56	237.81
6:00:00	294.96	-17.53	107.53	269.57
6:10:00	297.38	-18.47	108.47	302.87
6:20:00	299.82	-19.40	109.40	337.54
6:30:00	302.29	-20.30	110.30	373.41

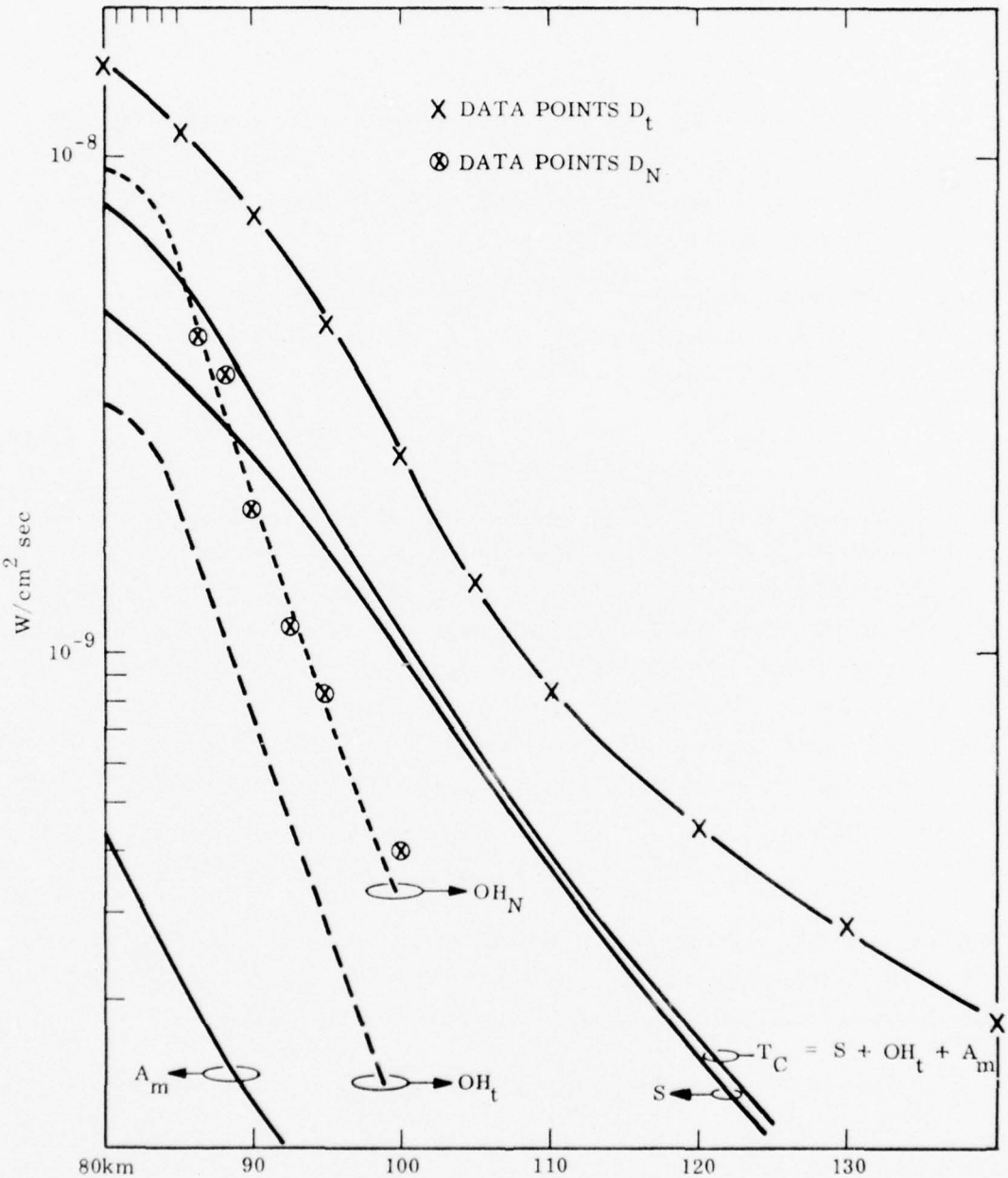

Fig. 15. The sunlit twilight 4.3 μm zenith radiance data points D_t and the night time dark data points D_N are compared with our predictions for the radiance components A_m which results from thermal collisions and the absorption of earthshine, OH_N a component due to $OH(v)^{VV}$ N_2 contribution which is obtained by reducing OH_N by a factor 3, S the component due to absorption of 4.3 and 2.7 μm sunlight by CO_2 which is followed by re-emission at 4.3 μm, and finally the sum $T_C = OH_t + S + A_m$ the total predicted radiance for the sunlit twilight case.

from absorption and re-emission of 4.3 μm sunlight by CO_2 in the bands j = 1 through 11, and from absorption of 2.7 μm sunlight followed with 96% probability by 4.3 μm fluorescent re-emission (Reference 8) in the bands j = 10 and 11, is the curve labelled S.

In order to calculate the contribution due to absorption and re-emission of 4.3 μm sunlight by CO_2 to the radiance component labelled S on Figure 15 we set (see KJ and also Reference 7).

$$\eta_j(z,t') = \sqrt{\pi}\, F_{s4}\, \lambda_D\, \sigma\, T_b \left(W_j\, \sigma\, N_{j\odot}(z,t')\right) . \qquad (15)$$

The quantity $N_{j\odot}(z,t')$ is the column density of [j] (where [j] is the ground state CO_2 specie for the jth CO_2 ν_3 band) along the line of sight from altitude point z to the sun at time t′. The quantities $N_{j\odot}(z,t')$ change in time due to the earth's rotation which causes the sun to set, since we measure t′ backwards in order to perform the integrals shown in equation (14) the sun actually rises as t′ increases. The $N_{j\odot}(z,t')$ decrease as t′ increases. An additional term to account for absorption of 2.7 μm sunlight which is followed by fluourescent re-emission at 4.3 μm must be added to the η_j for j = 10 and 11. This term is

$$\eta_{j2.7}(z,t') = \sqrt{\pi}\, F_{sj}\, \lambda_{Dj}\, \sigma_{2.7}\, T_b\, \sigma_{2.7}\, N_{1\odot}(z,t') \quad /G_j$$

where F_{sj} is the spectral solar irradiance near 2.7 μm (see KJ), λ_{Dj} is the 2.7 μm CO_2 e fold Doppler width, $\sigma_{2.7}$ is the Doppler line center cross section for absorption of 2.7 μm sunlight in the bands j = 10 and 11.

Since we are using the Q_w approximation $\eta_{NQ_w}(z,t')$ is given by

$$\eta_{NQ_w}(z,t') = \sum_{j=2}^{11} \eta_j(z,t')\, F_{Nj}\, G_j$$

For the matrix formulation (equations 2 through 4) of the Q_W approximation we set

$$\eta_i(t') = \eta_1(z_i, t')$$

$$\eta_{i+26}(t') = \eta_{NQ_W}(z_i, t')$$

With the inhomogeneous terms defined in this way we may turn the numerical crank to obtain the solutions f_i as explained in Section 3.4 above. The variation of $\eta_i(t')$ with t' is the result of variation in the quantities $N_{j\odot}(z,t')$ as t' is numerically stepped backwards from time 0 until the integrand in the numerical calculation of the integral

$$\eta_{ij} = \int_o^\infty dt' \, e^{-\lambda_j t'} \, \eta_i(t') \tag{16}$$

becomes negligible.

Here we briefly note that in a static approximation η_{ij} would be given by

$$\eta_{ij} \cong \eta_i(0) \, \lambda_j^{-1} \quad . \tag{17}$$

We shall focus our attention on this point later in the text since it turns out to be a point of interest for the planning of future experiments.

We return our attention to the rationalization of the 6 March 1975 data sets D_t and D_N that are shown on Figure 15. The radiance component due to absorption by CO_2 of sunlight at 4.3 and 2.7 μm and subsequent re-emission at 4.3 μm (the curve on Figure 15 marked S) is about a factor 2 to 4 less than the data D_t. By inspection of Figure 15 it is clear that the ratio of the curves D_t/S is by no means altitude independent over the region $80 < z < 110$ km. This means a simple adjustment of the radiometer calibration will not result in agreement between the data (curve D_t) and the sunlight driven component of our theoretical prediction, curve S.

There is still the sunlit component due to vibration transfer from $OH^{\pm}$ to N_2 (labelled on Figure 15 by curve OH_t) to contend with. According to

Gattinger (Reference 39) the twilight sunlit $OH^{\ddagger}$ column density component should be about a factor 3 less than the night time $OH^{\ddagger}$ column density.

The curve OH_N represents the night time 4.3 μm zenith radiance component due to vibration transfer from $OH^{\ddagger}$ to N_2. From the predictions of Gattinger (Reference 39) the sunlit twilight component of 4.3 μm zenith radiance due to vibration transfer from $OH^{\ddagger}$ to N_2 should be the night time component reduced by about a factor 3. Thus we believe the curve labelled OH_t on Figure 15 represents the component of the sunlit twilight 4.3 μm zenith radiance that is due to vibration transfer from $OH^{\ddagger}$ to N_2.

The sum of curves $S + OH_t + A_m$ is our prediction then for the total CO_2 4.3 μm zenith radiance for the sunlit twilight case. This sum is labelled T_c.

The ratio of our theoretical prediction T_c to the data D_t is essentially a constant value 0.5 in the region $80 < z \lesssim 110$ km. We tried to increase the predicted radiance value by doubling the amount of CO_2 in our model but since the sun is below local horizontal and since the CO_2 is optically thick along the path from the sun to the point z in the region $80 < z < 110$ km doubling the amount $[CO_2]$ resulted in increasing S by just a factor of approximately 1.2 at 80 km, increasing gradually to 1.4 at 100 km, and then more slowly to 1.5 at 140 km. Since a factor x2 change in our model for $[CO_2]$ does not appreciably change our predicted sunlit driven radiance value, it is our preliminary inclination to suggest that the absolute radiometer calibration may be off by a factor 2 so that the data sets D_t and D_N may be reduced by a factor of 2. Communication with D. J. Baker established that such a possibility is not inconceivable.

Such a reduction of the data by a factor of 2 achieves (1) an excellent fit of the data D_t and theory T_c for $80 < z \lesssim 110$ km, (2) allows us to reduce E_{Tv} to 0.177 ergs/cm^2 sec of vibration transfer from $OH^{\ddagger}$ to N_2 in order to fit OH_N to the night time data D_N.

We are not concerned at this time that the ratio T_c/D_t is not constant for $z \gtrsim 110$ km. To accurately compute S in this region requires an accurate

model for the temperature profile T(z), as well as the computational facility to deal with the broadening of the CO_2 bands and lines which is occurring in this region due to the rapid increase in atmospheric temperature which occurs for z > 100 km. The band and line broadening should tend to increase the radiance over what we predict for z > 100 km. For the computation we show on Figure 15 we used a model with an exospheric temperature of 1000° K.

Before closing out this section we call attention to Figure 16. On Figure 16 we show two calculations for the sunlight driven component of our predictions of the 4.3 μm zenith radiance appropriate for the sunlit twilight case. The total complete sunlit driven component is the sum of the radiance in bands j = 1 through 11 and is labelled ΣR_j. We also show the radiance component R_1 in the strong band and the radiance in the sum of the fluorescent bands $R_{10} + R_{11}$. The two calculations apply for η_{ij} calculated via equation (16) (a dynamic calculation) or for η_{ij} calculated by equation (17) (a static calculation). Results of the dynamic calculation are indicated by the solid curves on Figure 16, and results of the dynamic calculation are indicated by the dashed curves on Figure 16.

The fluorescent component $R_{10} + R_{11}$ is prompt and is therefore identical regardless of whether η_{ij} is calculated via equations (16) or (17). We see that R_1 is 40% reduced near z ≃ 80 km in the static case compared to the dynamic case. The difference in ΣR_j in the static versus the dynamic case is mostly due to the static versus dynamic effects on R_1, the radiance in the strong band.

From Figure 16 we learn that the weak bands $\sum_{j=2}^{11} R_j$ are just as strong, or stronger than the strong band R_1 for the altitude region where data were obtained in the sunlit twilight shot on 6 March 1975. We also see that conditions of solar illumination are changing slowly enough so that the dynamic effects are so mild that they will not be dramatically manifest in the data. Since conditions of twilight solar illumination seem to be changing slowly compared to $\tau(z)$ the N_2^+ residence time it appears that twilight experiments are perhaps not a conclusive way to use temporal variations of solar

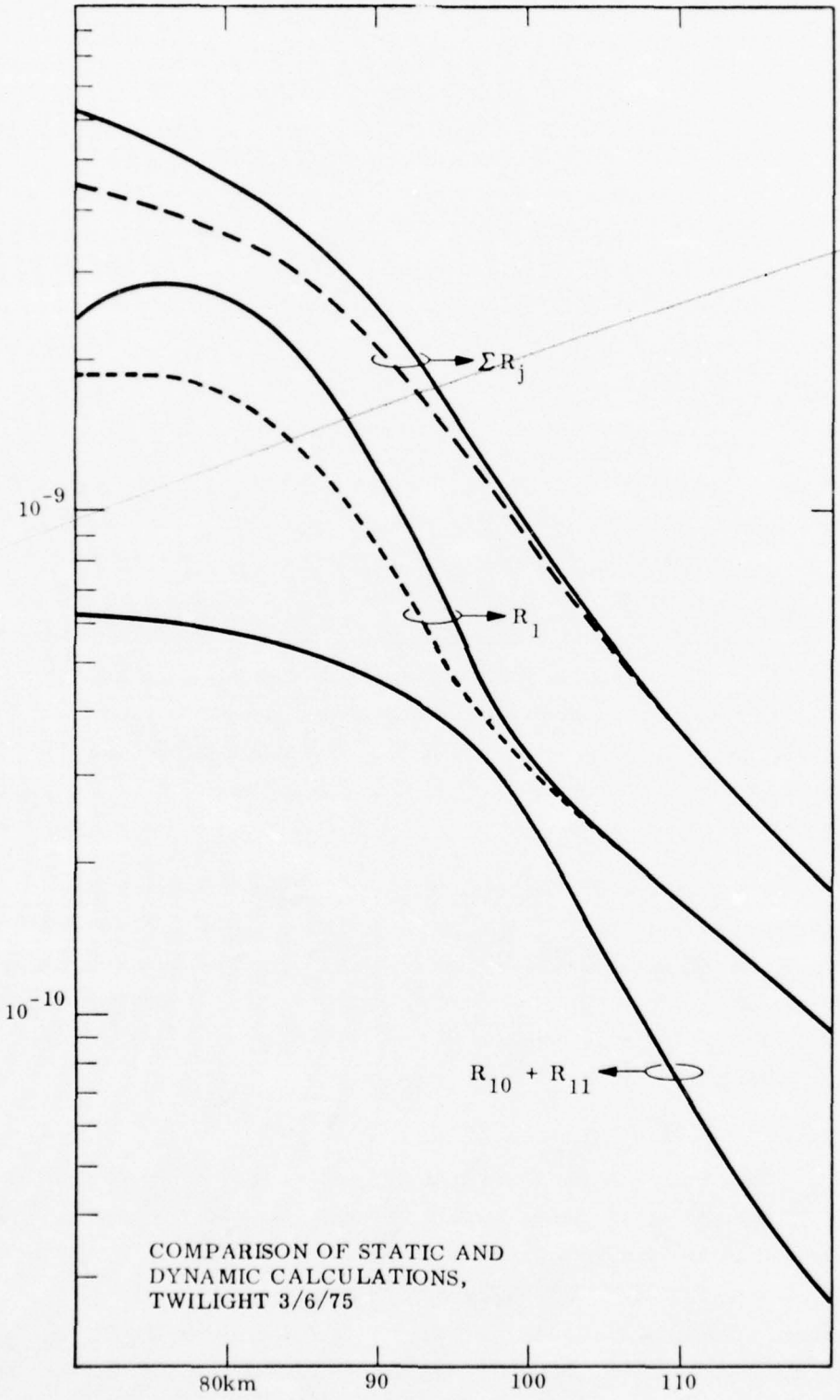

Figure 16. A comparison of static and dynamic calculations, twilight 6 March 1975.

illumination to test our time dependent theory of upper atmospheric non-LTE 4.3 μm emissions by CO_2. Perhaps the more rapid variation of solar illumination, which presumably occurs in a lunar eclipse of the sun, might be rapid enough that time dependent effects in data taken under eclipse conditions would be dramatic enough to be easily identified.

3.6 Summary of Evidence for $OH^{\ddagger} \xrightarrow{VV} N_2$ Driven 4.3 μm Airglow

In our discussions of the data received 27 March 1973, 11 April 1974, 25 February 1974 and 6 March 1975 we have pointed out that near 80 km altitude there are features in these data that can be explained as a manifestation of our postulated $OH^{\ddagger} \xrightarrow{VV} N_2$ driven CO_2 4.3 μm airglow. The amounts of vibrational energy E_{Tv} which need to be transferred to N_2 to explain the features are listed below:

Data Set		E_{TV} (units, ergs/cm^2 sec)
27 March 1973	Downleg	0.22
11 April 1974		0.08
25 February 1974	Upleg	0.13
6 March 1975	Sunlit Twilight	0.06
6 March 1975	Night Time	0.18

In case of the 6 March 1975 data the $OH^{\ddagger} \xrightarrow{VV} N_2$ driven component had to have the same diurnal variation as is predicted for $OH^{\ddagger}$ production in order to achieve a consistent analysis for these data.

The $OH^{\ddagger} \xrightarrow{VV} N_2$ mechanism seems promising enough to persue further in order to achieve firm verification.

Analytically this would involve an effort to re-examine the data obtained 9 March 1972 and the upleg data obtained 27 March 1973 for further evidence of the $OH^{\ddagger} \xrightarrow{VV} N_2$ driven CO_2 4.3 μm airglow. Any ground, rocket, or aircraft based OH airglow data which have been taken coincidentally with the 4.3 μm data should be carefully examined for correlated effects. First order considerations would indicate the brightness of the $OH^{\ddagger}$ airglow and the value E_{Tv} might be expected to correlate for example.

Future 4.3 μm rocket shots should also have instrumentation to measure OH airglow, ideally this instrumentation should be designed to measure as closely as is possible the altitude dependence of the population OH(v) for each value of v in the range $1 \leq v \leq 9$.

3.7 Evaluation of Data Obtained 12 March 1975

On Figure 17 the curve T_c shows our predicted 4.3 μm zenith radiance profile for the upleg of the 12 March 1975 shot which was launched at 7:48:10.035 UT. T_c is the sum of 3 components, these are the curves labelled A_m, OH and A_u.

The curve A_m is the component due to absorption of earth shine and thermal collisions. In order to compute A_m we used ASL rocket data obtained up to $z \simeq 60$ km (Reference 34), we joined this data smoothly to a 195°K March 65° N model mesopause temperature near z = 90 km.

The curve OH is a guess for the $OH^{\pm VV}\rightarrow N_2$ airglow component of the CO_2 4.3 μm radiance appropriate for this event. The value $E_{Tv} = 0.08$ ergs/cm^2 sec was used in computing the OH component. Comparison with the 4.3 μm zenith radiance data will provide a better means for establishing what value is most appropriate for E_{Tv} for the 12 March 1975 upleg, we have not as yet seen these data, however.

The curve A_u is our prediction for the auroral contribution to the upleg 12 March 1975 4.3 μm zenith radiance data. This curve was computed via our BRIM model. Preliminary scanning photometer red and blue (4278 Å) data taken near upleg penetration were provided by Sears (Reference 40) for input for the BRIM computation. These data are listed in Table 5 below. These data have been corrected for attenuation via the averaged model in Reference 32. Use of the averaged model may have introduced an underestimate in the attenuation correction since total deposition $\int dz\, q$ that we deduce from preliminary radar data on $n_e(z)$ at 7:47 UT (Reference 41) is nearly a factor x3 larger than we infer from the blue photometric data. On the other hand the difference

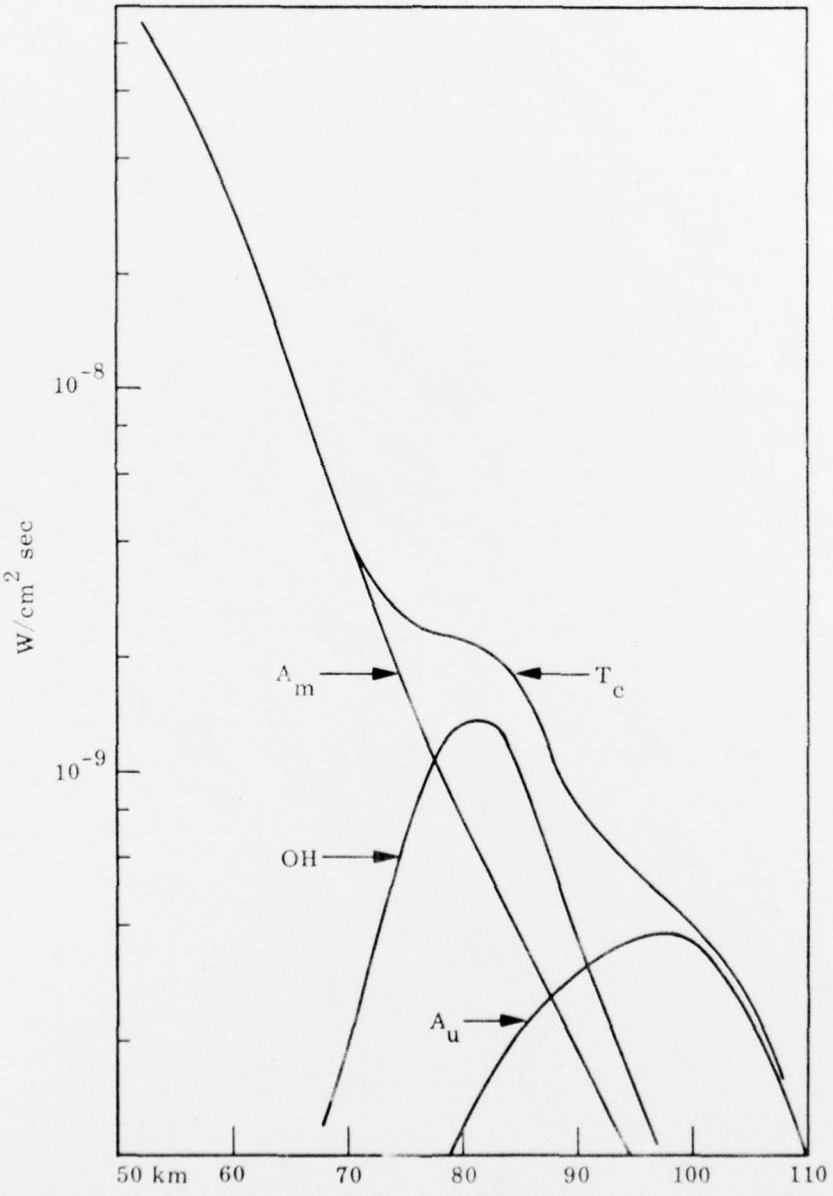

Figure 17. Curve T_c is our preliminary prediction for the 12 March 1975 upleg 4.3 μm zenith radiance profile.

Table 5. The ground based (Reference 40) red 6300 Å histories $4\pi I_R(t')$ and $4\pi I_B(t')$ for the 12 March 1975 upleg analysis are listed below. These data have been corrected for atmospheric extinction via the averaged model (Reference 32).

	kR	
t′ (min)	$4\pi I_R$	$4\pi I_B$
-.41	.43	1.60
1.25	.67	2.10
2.25	.55	2.06
3.91	.35	0.81
4.91	.50	2.0
6.58	.29	0.43
7.58	.34	0.18
9.25	.22	6.86
10.25	.23	6.53
11.90	.17	6.16
12.90	.17	6.16

in $\int dz\ q$ deduced from the two preliminary data sets may simply result from the differing fields of view and viewing aspect of the radar and the scanning photometer. Data analysis is too preliminary at this point for any definite conclusions regarding the differences in $\int dz\ q$ obtained by the two methods. In either case the radar and photometric data both show that $d/dz\ q(z) = 0$ should occur at 114 km. A value $\epsilon = 10$ (N_2^+/ionization) was used in the computation of A_u. It is conceivable that A_u could be $\simeq 5$ times larger in magnitude than our preliminary calculation shown on Figure 17. A factor 3 might come from utilization of an input model normalized so that $\int dz\ q$ agrees with the radar data, another factor 1.67 could come from increasing ϵ to 16.7 (N_2^+/ionization).

4.0 CONCLUSIONS

One of the tasks of our project was to develop the facility to numerically solve the exact time dependent plane parallel radiation transport equations which describe the CO_2 4.3 μm aurora. We discuss the successful performance of this task in Section 2.0 above. In performing this task we found that inclusion of the weak CO_2 ν_3 bands has a profound effect on the time dependence and on the absolute magnitude of CO_2 4.3 μm emission in the altitude region $z \leq 90$ km. This profound change is illustrated by comparing the calculation for $N_2^{\ddagger}$ residence time $\tau(z)$ in which the weak CO_2 ν_3 bands are ignored (this is the curve labelled EFA, $Q_W = 0$ on Figure 1) with the calculations for $\tau(z)$ in which the weak CO_2 ν_3 bands are accounted for, these are the curves labelled EFA, Q_W and EFA 12 x 12 on Figure 1. Similarly, a significant fraction of the CO_2 4.3 μm zenith radiance observed at altitudes $z < 80$ km will occur in the weak bands. Results shown on Figures 2 and 3 above illustrate this point.

A second task was to use the facility to numerically solve the exact time dependent transport (TDT) equation to evaluate the data obtained 24 and 27 March 1973, 25 February 1974, 11 April 1974, 6 March 1975 and 12 March 1975.

A better fit between 24 March 1973 data and theory in the $z < 90$ km region was achieved by using our improved TDT calculational facility as compared to the fit to those data we had reported previously (CRL0334) which was achieved by application of a calculational facility which employed the stationary time dependent approximation (STDA) to the TDT formulation. The earlier method had neglected the weak CO_2 ν_3 bands and this was the principal reason that better agreement with the data was achieved by our improved TDT facility in the region $z < 90$ km. For $z > 90$ km the fits to the 24 March 1973 data that were achieved by the TDT and STDA facilities were essentially identical as might be expected.

There were no data obtained 24 March 1973 for $z < 80$ km. Since the really spectacular effects of the weak CO_2 ν_3 bands only begin to show up for $z > 80$ km, no such spectacular effects were evident in the data. Typically auroral data

will not manifest these dramatic effects since auroral deposition occurs for $z > 90$ km. Absorption by intervening atmospheric CO_2 of CO_2 4.3 μm emission in the region of auroral depositions renders the auroral 4.3 μm zenith radiance for $z < 80$ km quite weak in comparison to other sources of CO_2 4.3 μm zenith radiance in this altitude region. This means that measurements of auroral 4.3 μm CO_2 zenith radiance are not a very effective way to verify the spectacular effects of the weak CO_2 ν_3 bands that the TDT theory predicts will occur for $z < 80$ km. For DNA interest, significant energy deposition occurs in the region $z < 80$ km as the result of high altitude detonations.

The 27 March 1973 downleg ($60 < z < 100$ km) data were taken at a place where no appreciable auroral deposition had occurred in the previous 45 minutes at least. We used the TDT facility to determine that the feature in these data in the 70 to 80 km altitude range (see Figure 5 below) could not be the decaying remnant of an intense 4.3 μm aurora which may have been present more than 45 minutes prior to downleg penetration. A similar feature was noted in evaluation of the 11 April 1974 data which were purposefully obtained on an evening when there was no auroral activity. In analysis of these data we determined that the mechanism

$$OH(v) + N_2 \rightarrow OH(v-1) + N_2^{\ddagger}$$

is probably the mechanism most likely to be responsible for the feature near 80 km which is noted in the 11 April 1974 data and, by inferrence, for the similar feature noted in the 27 March 1973 downleg data. A total vibrational energy transfer E_{TV} from $OH(v)$ to N_2 of about 0.078 and 0.22 ergs/cm^2 sec is required, respectively, to explain these features in the 11 April 1974 data and in the 27 March 1973 downleg data.

The 25 February 1974 data were obtained in the presence of an active moving auroral arc which produced large auroral components of 4.3 μm zenith radiance on both the upleg and downleg.

For evaluation of these data we developed a facility to utilize ground based scanning photometer blue (4278 Å) and red (6300 Å) data in order to develop an energy input model (BRIM) appropriate for the upleg and downleg

penetration points. The total column deposition $\int dz\ q(z,t')$ is at some time t' prior to penetration obtained from the absolute magnitude of the blue data and the approximate altitude dependence $q(z,t')$ is obtained from the red to blue ratio. Corrections for atmospheric attenuation must be applied to the ground based photometric data.

In practice, correction of the aerosol component of attenuation may be very difficult to apply accurately. Nevertheless, we were able to consistently model both the upleg and downleg 4.3 μm aurora data sets on the basis of upleg and downleg energy deposit histories $q(z,t')$ constructed via the BRIM facility. The aerosol corrections to the photometric data were based on an averaged atmospheric model.

The values $15 \leq \varepsilon \leq 20$ ($N_2^{\ddagger}$/ionization) were necessary to fit both the upleg and downleg 4.3 μm data. The addition of a component of 4.3 μm radiance due to transfer of vibration from OH(v) to N_2 of about $0.09 < E_{Tv} < 0.14$ ergs/cm^2 sec resulted in a much better fit to the upleg data than would have been achieved for $E_{Tv} = 0$. Due to rocket tipover at $z = 85$ km on the downleg we did not attempt to analyze the downleg data for $z < 85$ km in terms of the OH(v) vs N_2 mechanism.

In our discussion of the 25 February 1974 data we noted a side point with regard to the possibility of CO_2 2.8 μm emission with a long (1 to 5 minute) response time period and with $N_2^{\ddagger}$ as energy the storage mechanism. To get within a factor of about 10 of what seems to be the required magnitude of the 2.7 μm radiance requires that the vibration transfer rate constant for the reactions

$$CO_2 \begin{Bmatrix} 101 \\ 021 \end{Bmatrix} + N_2 \overset{k_f}{\rightleftarrows} CO_2 \begin{Bmatrix} 100 \\ 020 \end{Bmatrix} + N_2^{\ddagger}$$

should be 10^3 larger than for the reaction

$$CO_2\ (001) + N_2 \overset{k_2}{\rightleftarrows} CO_2\ (000) + N_2^{\ddagger} \quad .$$

It seems unlikely that k_f should differ significantly from k_2, but the possibility may warrant further attention.

Next we applied our TDT theory for evaluation of data obtained 6 March 1975 on two rocket shots, one into the sunlit twilight atmosphere and the other into the night time dark atmosphere. There was no significant auroral activity. A consistent evaluation was achieved on the basis of two airglow mechanisms. One is the $OH(v) \overset{VV}{\rightarrow} N_2$ mechanism. The other is the absorption of 4.3 and 2.7 μm sunlight by CO_2 followed by emission at 4.3 μm. The data indicated that the sunlit twilight component of 4.3 μm radiance due to the $OH(v) \overset{VV}{\rightarrow} N_2$ mechanism must be about a factor 3 less than the night time component, in accord with accepted theory for the diurnal dependence of the OH(v) production. Values of $E_{Tv} \cong .06$ and .18 ergs/cm^2 sec are required in the sunlit and dark cases respectively. The evaluation indicated that conditions of solar illumination are not changing rapidly enough during high latitude twilight to produce dramatically evident time dependent effects. Perhaps solar illumination would vary rapidly enough to produce such effects in low latitude twilight or in ecliptic conditions.

On 12 March 1975, 4.3 μm zenith radiance data were obtained in a broad diffuse aurora. We used preliminary photometric data as input for the BRIM model to obtain $q(z,t')$ for the upleg and then input $q(z,t')$ to the TDT computation to obtain a preliminary prediction for the auroral 4.3 μm zenith radiance component of the 12 March 1975 upleg data. We also predicted that there will be some manifestation of the $OH(v) \overset{W}{\rightarrow} N_2$ mechanism in these data.

5.0 ACKNOWLEDGEMENTS

The success of the work reported here was crucially dependent on the generous advice and discussion provided by colleagues. In particular, discussions with A. T. Stair, D. J. Baker, R. D. Sears and T. C. James were instrumental in the formulation of an $OH(v) + N_2 \rightarrow OH(v-1) + N_2^{\ddagger}$ concept for 4.3 μm airglow. The formulation of the BRIM capability would not have been possible under this contract without the valuable assistance of R. D. Sears. All of the people that we dealt with went out of their way to provide information pertinent to successful performance of the contractual tasks. To name just a few these people included Maj. L. Doan, C. A. Blank, A. T. Stair, J. C. Ulwick, Ned Wheeler, W. G. Grieder, R. D. Sears, T. C. James, R. Gunton, W. E. Francis, D. J. Baker. G. A. Ware, K. D. Baker, R. O. Olsen, H. Mitchell and M. J. Baron.

6.0 REFERENCES

1. Kumer, J. B.; "Analysis of 4.3 μm ICE CAP Data," Air Force Cambridge Research Laboratories Technical Report, AFCRL-TR-74-0334, 1974.

2. Stair, A. T., J. C. Ulwick, K. D. Baker and D. J. Baker; "Rocketborne Observations of Atmospheric Infrared Emissions in the Auroral Region," Atmospheres of Earth and Planets, ed. B. M. McCormac, published by D. Reidel, Dordrecht, Holland, 1975.

3. Kumer, J. B.; "Summary Analysis of 4.3 μm Auroral Data," Atmospheres of Earth and Planets, ed. B. M. McCormac, published by D. Reidel, Dordrecht, Holland, 1975.

4. Dickinson, R. E., "Method of Parameterization for Infrared Cooling between Altitudes of 30 and 70 kilometers," J. Geophys. Res. 78, 4451, 1973.

5. McClatchey, R. A., W. S. Benedict, S. A. Clough, D. E. Burch, R. F. Coffee, K. Fox, L. S. Rothman and J. S. Garing, "AFCRL Atmospheric Absorption Line Parameters Compilations," AFCRL-TR-73-0096, 1973.

6. Kumer, J. B., and T. C. James; "CO_2 (001) and N_2 Vibrational Temperatures in the $50 \leq z \leq 130$ km Altitude Range," J. Geophys. Res. 79, 638, 1974.

7. Kumer, J. B., "CO_2 and N_2 Vibrational Temperatures, 40 to 140 km," to be submitted to J. Geophys. Res., 1976.

8. James, T. C., and J. B. Kumer; "Fluorescence of CO_2 near 4.3 μm: Application to Daytime Limb Radiance Calculations," J. Geophys. Res. 78, 1973.

9. Taylor, R. L., "Energy Transfer Processes in the Stratosphere," Can. J. Chem., 52, 1436, 1974.

10. Taylor, R. L., Private Communication, 1975.

11. Kumer, J. B.; "Theory of the CO_2 4.3 μm Aurora and Related Phenomena," submitted to J. Geophys. Res., 1976.

12. Tarr, P. W., and D. H. Archer, "Auroral Simulation Studies in Support of ICE CAP and EXCEDE," HAES Report No. 24, DNA3785F, September 1975.

13. Baron, M. J., and N. J. Chang, "ICE CAP '73a - Chatanika Radar Results," HAES Report No. 15, DNA3531T, April 1975.

14. Ulwick, J. C., and A. T. Stair, Jr., "ICE CAP and EXCEDE Measurements," Minutes of the 4th ARPA sponsored Strategic Space Symposium held 23 September 1975 at the U.S. Naval Postgraduate School, Monterey, Calif.

15. Kumer, J. B., "Report on the USU Subcontract BB73 Calibration by Thermal Atmospheric Radiance (CTAR)," draft final report on Utah State University Subcontract SC-75-019 authorized by Government Contract F19628-73-C-0048, 1975b.

16. Wheeler, N., private communication of preliminary 11 April 1974 4.3 μm zenith radiance data, 1976.

17. Wheeler, N., "Rocket Borne Spectral Measurements of Atmospheric Infrared Emissions During Quiet Conditions in the Auroral Zone," 1976.

18. Olsen, R. O., private communication of meteorological rocket data up to 60 km altitude for the date 11 April 1974, 1974.

19. Groves, G. V.; "Atmospheric Models," Air Force Cambridge Research Laboratories Technical Report, AFCRL-TR-70-1261, 1970.

20. Baker, D. J.; "A Review of the OH Airglow," draft version as of August 1976.

21. Rogers, J. W., R. E. Murphy, A. T. Stair, Jr., J. C. Ulwick, K. D. Baker and L. L. Jensen; J. Geophys. Res. 78, 7023, 1973.

22. Baker, D. J.; private communication relating total OH $\Delta V = 2$ sequence emission measured with filter band pass as reported in Reference 21, August 1976.

23. Charters, P. E., R. G. Macdonald and J. C. Polanyi; Appl. Optics 10, 1747, 1971.

24. Streit, G. E., and H. S. Johnston; J. Chem. Phys. 64, 95, 1976.

25. Mies, F. H.; J. Mol. Spectry. 53, 150, 1974.

26. Grieder, W., and A. T. Stair, Jr.; "Short Wavelength Infrared Spectral Measurements in an IBC-II Aurora Using a Rocketborne CVF Spectrometer," 1976.

27. Perreault, P. D., and M. J. Baron; "ICE CAP '74 - Chatanika Radar Results," DNA3871T, October 1975.

28. Sears, R. D.; "Ionospheric Irregularities: Auroral Motions and Drifts," DNA3514F, April 1975.

29. Ware, G. A., R. J. Huppi, A. J. Steed, B. V. Bartschi, R. D. Briscoe and R. J. Bell; "Ground Support Data Report for Black Brant 18.219-1 Flight of 25 February 1974," draft report submitted to AFCRL on 2 September 1974.

30. Rees, M. H., and D. Luckey; J. Geophys. Res. 79, 5181, 1974.

31. Rees, M. H.; Planet. Space Sci. 11, 1209, 1963.

32. Elterman, L.; "UV, Visible and IR Attenuation for Altitudes up to 50 km, 1968," AFCRL-68-0153, Environmental Research Papers No. 285, April 1968.

33. Wickwar, V. B., M. J. Baron and R. D. Sears; J. Geophys. Res. 80, 4364, 1975.

34. Olsen, R. O.; private communication of meteorological rocket data on atmospheric temperature and density for the 25 February 1974, 11 April 1974, 6 March 1975 and 12 March 1975 events, June 1976.

35. Mitchell, H.; "Gap Between DNA Data and Theory at 2.8 μm, Possible Explanation," Memo from H. Mitchell, 13 October 1976.

36. Ware, G. A., and D. J. Baker; private communication of solar zenith angle and refraction corrected slant height as a function of time for the 6 March 1975 event.

37. Ware, G. A., and D. J. Baker; "OH Rotational Temperatures at Auroral Latitudes," EOS 57, 301, 1976.

38. Gattinger, R. L.; Ann. Geophys. 25, 825, 1969.

39. Sears, R. D.; private communication of attenuation corrected red and blue (4278 Å) scanning photometer data obtained 12 March 1975, October 1976.

40. Baron, M. J.; private communication of preliminary radar data for 12 March 1975, provided to R. D. Sears.

DISTRIBUTION LIST

DEPARTMENT OF DEFENSE

Director
Defense Advanced Rsch. Proj. Agency
ATTN: Lieutenant Colonel W. A. Whitaker
ATTN: STO, Captain J. Justice
ATTN: Major Gregory Canavan

Defense Documentation Center
Cameron Station
12cy ATTN: TC

Director
Defense Nuclear Agency
ATTN: STSI, Archives
ATTN: RAAE, Harold C. Fitz, Jr.
ATTN: RAAE, Major John Clark
ATTN: DDST
3cy ATTN: RAAE, Charles A. Blank
3cy ATTN: STTL, Tech. Library

Dir. of Defense Rsch. & Engineering
ATTN: DD/S&SS, Daniel Brockway

Commander
Field Command
Defense Nuclear Agency
ATTN: FCPR

Chief
Livermore Division Fld. Command DNA
Lawrence Livermore Laboratory
ATTN: FCPRL

DEPARTMENT OF THE ARMY

Commander/Director
Atmospheric Sciences Laboratory
U.S. Army Electronics Command
ATTN: DRSEL-BL-SY-S, F. E. Niles

Commander
Harry Diamond Laboratories
2cy ATTN: DRXDO-NP

Commander
U.S. Army Nuclear Agency
ATTN: MONA-WE

DEPARTMENT OF THE NAVY

Chief of Naval Research
ATTN: Code 464

Commander
Naval Electronics Laboratory Center
ATTN: Code 2200, Verne E. Hildebrand
ATTN: Code 2200, Ilan Rothmuller

Director
Naval Research Laboratory
ATTN: Code 770, Jack D. Brown
ATTN: Code 2600, Tech. Lib.

DEPARTMENT OF THE NAVY (Continued)

Director
Naval Research Laboratory (Continued)
ATTN: Code 7127, Charles Y. Johnson
ATTN: Douglas P. McNutt
ATTN: Code 7750, Darrell F. Strobel
ATTN: Code 7750, Paul Julienne
ATTN: Code 7700, Timothy P. Coffey

Commander
Naval Surface Weapons Center
ATTN: Code WA501, Navy Nuc. Prgms. Off.

DEPARTMENT OF THE AIR FORCE

AF Geophysics Laboratory, AFSC
ATTN: LKB, Kenneth S. W. Champion
ATTN: OP, John S. Garing
ATTN: OPR, Alva T. Stair

AF Weapons Laboratory, AFSC
ATTN: SUL
ATTN: DYT, LtCol Don Mitchell

Commander
ASD
ATTN: ASD-YH-EX, LtCol Robert Leverette

SAMSO/SZ
ATTN: SZJ, Major Lawrence Doan

ENERGY RESEARCH & DEVELOPMENT ADMINISTRATION

Division of Military Application
ATTN: Doc. Con. for Major D. A. Haycock

Los Alamos Scientific Laboratory
ATTN: Doc. Con. for R. A. Jeffries

OTHER GOVERNMENT AGENCIES

Department of Commerce
Office of Telecommunications
Institute for Telecom Science
ATTN: William F. Utlaut
ATTN: Glenn Falcon

DEPARTMENT OF DEFENSE CONTRACTORS

Aerodyne Research, Inc.
ATTN: F. Bien
ATTN: M. Camac

Aerospace Corporation
ATTN: R. D. Rawcliffe
ATTN: Harris Mayer
ATTN: R. Grove
ATTN: T. Taylor

General Electric Company
TEMPO-Center for Advanced Studies
ATTN: Warren S. Knapp
5cy ATTN: DASIAC, Art Feryok

DEPARTMENT OF DEFENSE CONTRACTORS (Continued)

University of Denver
Colorado Seminary
Denver Research Institute
ATTN: Sec. Officer for Mr. Van Zyl
ATTN: Sec. Officer for David Murcray

General Research Corporation
ATTN: John Ise, Jr.

Geophysical Institute
University of Alaska
ATTN: T. N. Davis
3cy ATTN: Neal Brown

Honeywell Incorporated
Radiation Center
ATTN: W. Williamson

Institute for Defense Analyses
ATTN: Hans Wolfhard
ATTN: Ernest Bauer

Lockheed Missiles and Space Company
ATTN: John Kumer
ATTN: John B. Cladis, Dept. 52-12
ATTN: Billy M. McCormac, Dept. 52-54
ATTN: Tom James
ATTN: J. B. Reagan, D/52-12
ATTN: Martin Walt, Dept. 52-10
ATTN: Richard G. Johnson, Dept. 52-12
ATTN: Robert D. Sears, Dept. 52-14

Mission Research Corporation
ATTN: P. Fischer
ATTN: D. Archer

Photometrics, Inc.
ATTN: Irving L. Kofsky

Physical Dynamics, Inc.
ATTN: Joseph B. Workman

Physical Sciences, Inc.
ATTN: Kurt Wray

DEPARTMENT OF DEFENSE CONTRACTORS (Continued)

R & D Associates
ATTN: Forrest Gilmore
ATTN: Robert E. Lelevier

R & D Associates
ATTN: Herbert J. Mitchell

The Rand Corporation
ATTN: James Oakley

Science Applications, Inc.
ATTN: Daniel A. Hamlin

Space Data Corporation
ATTN: Edward F. Allen

Stanford Research Institute
ATTN: M. Baron
ATTN: Ray L. Leadabrand
ATTN: Walter G. Chesnut

Stanford Research Institute
ATTN: Warren W. Berning

Technology International Corporation
ATTN: W. P. Boquist

Utah State University
ATTN: Doran Baker
ATTN: C. Wyatt
ATTN: D. Burt
ATTN: Kay Baker

Visidyne, Inc.
ATTN: J. W. Carpenter
ATTN: Henry J. Smith
ATTN: T. C. Degges
ATTN: Charles Humphrey
ATTN: William Reidy
ATTN: L. Katz